Published in final edited form as:
Geochim Cosmochim Acta. 2014 February 15; 127: 326–347. doi:10.1016/j.gca.2013.11.030.

Heavy noble gases in solar wind delivered by Genesis mission

Alex Meshik[a,*], **Charles Hohenberg**[a], **Olga Pravdivtseva**[a], and **Donald Burnett**[b]

[a]Department of Physics, Washington University, 1 Brookings Drive, Saint Louis, MO 63130, USA

[b]Geological and Planetary Sciences, California Institute of Technology, Pasadena, CA 91125, USA

Abstract

One of the major goals of the Genesis Mission was to refine our knowledge of the isotopic composition of the heavy noble gases in solar wind and, by inference, the Sun, which represents the initial composition of the solar system. This has now been achieved with permil precision: $^{36}Ar/^{38}Ar = 5.5005 \pm 0.0040$, $^{86}Kr/^{84}Kr = .3012 \pm .0004$, $^{83}Kr/^{84}Kr = .2034 \pm .0002$, $^{82}Kr/^{84}Kr = .2054 \pm .0002$, $^{80}Kr/^{84}Kr = .0412 \pm .0002$, $^{78}Kr/^{84}Kr = .00642 \pm .00005$, $^{136}Xe/^{132}Xe = .3001 \pm .0006$, $^{134}Xe/^{132}Xe = .3691 \pm .0007$, $^{131}Xe/^{132}Xe = .8256 \pm .0012$, $^{130}Xe/^{132}Xe = .1650 \pm .0004$, $^{129}Xe/^{132}Xe = 1.0405 \pm .0010$, $^{128}Xe/^{132}Xe = .0842 \pm .0003$, $^{126}Xe/^{132}Xe = .00416 \pm .00009$, and $^{124}Xe/^{132}Xe = .00491 \pm .00007$ (error-weighted averages of all published data). The Kr and Xe ratios measured in the Genesis solar wind collectors generally agree with the less precise values obtained from lunar soils and breccias, which have accumulated solar wind over hundreds of millions of years, suggesting little if any temporal variability of the isotopic composition of solar wind krypton and xenon. The higher precision for the initial composition of the heavy noble gases in the solar system allows (1) to confirm that, exept ^{136}Xe and ^{134}Xe, the mathematically derived U–Xe is equivalent to Solar Wind Xe and (2) to provide an opportunity for better understanding the relationship between the starting composition and Xe-Q (and Q-Kr), the dominant current “planetary” component, and its host, the mysterious phase-Q.

1. INTRODUCTION

Samples containing the Solar Wind (SW), captured by Genesis Mission collectors (http://genesismission.jpl.nasa.gov/; Burnett et al., 2003; Jurewicz et al., 2003), became available for laboratory analyses in early 2005. However, it took more than 5 years of refining the analytical capabilities for results for of all noble gases to emerge. These efforts are continuing and the accuracy of solar wind isotopic analyses is increasing. The low concentrations of SW Kr and Xe in the Genesis collectors required development of a new sensitive multiple multiplier mass-spectrometer and an intricate low-blank laser extraction system capable of handling the large amounts of hydrogen, the dominant solar wind component.

*Corresponding author. Tel.: +1 314 935 5049. am@physics.wustl.edu (A. Meshik).

Associate editor: Gregory F. Herzog

The light noble gases are abundant in the SW, so little modification to current mass spectrometry was needed to perform these isotopic analyses, with the exception of changes needed to handle the large concentrations of solar wind hydrogen. He and Ne isotopes in Genesis SW collectors have been independently measured by groups in St. Louis (Meshik et al., 2007; Mabry, 2009), in Zürich (Grimberg et al., 2006, 2007, 2008; Heber et al., 2009) and recently in Minnesota (Pepin et al., 2012). Although some disagreements between these analyses are still present, they all confirm the isotope fractionation expected during implantation of uniform-velocity SW-ions – a process predicted by a number of theoretical calculations (Tamhane and Agrawal, 1978) and semi-empirical simulations (c.f. TRIM, Becker, 1998; Pepin et al., 2012). With solar wind ions bound to the solar magnetic field, they all are implanted at constant velocity, not energy, making isotope ratios heavier with implantation depth. However, in spite of this knowledge and those studies, the depth dependent isotope fractionation with constant velocity implantation was largely overlooked for more than two decades. Instead, an alternative concept of deeply implanted SEP noble gas component dominated the noble gas literature, including scholarly books by Ozima and Podosek (2002) and “Noble Gases in Geochemistry and Cosmochemistry” (2002). Now, after analyses of Ne in Genesis SW-collectors (Grimberg et al., 2006) and the Ar depth profiles reported in this study, the controversial concept of SEP noble gas component can be discarded.

Heavy noble gases are far less abundant in the SW, and existing noble gas mass-spectrometers are not well suited for the precise isotope analyses of the small amounts of Xe (~10^6 SW atoms/cm^2) and Kr (~10^7 SW at/cm^2) that accumulated in the Genesis collectors during the 27 months of exposure to the SW. Reaching the precision set by the Genesis Mission goals would have required that an unrealistically large surface area (~10 cm^2) of SW-collector be degassed in a reasonable time.

We already reported our preliminary heavy noble gas results in aluminum Genesis SW collectors (Meshik et al., 2012). Here we present our final (as of today) results independently verified by other laboratories using different SW-collectors and employing different analytical techniques. Based on this comparison we suggest the best current estimates for all Ar, Kr and Xe isotopes in the SW delivered by Genesis Mission.

2. EXPERIMENTAL

2.1. Mass spectrometry

At the time when Genesis spacecraft was on the launch pad we had in the laboratory our sensitive ion-counting mass spectrometer SuperGnome (Hohenberg, 1980), which was developed for high-precision measurements of low-abundance noble gases and has excelled through the years as a reliable Xe instrument. It achieves its 100% ion transmission by means of a low electric field gradient in the ion extraction region which makes identical paths for every isotope, a 90 degree small gap magnetic sector with minimum fringe field effects and a discrete BeCu dynode electron multiplier. The resulting instrument has an excellent ion transmission with no loss on any defining slits and an almost 100% counting efficiency, all of which combine to make a low-memory instrument essentially free of isotope mass discrimination with single ion detection. However, since there is only one

multiplier and Kr and Xe cannot be cleanly separated cryogenically, the only way to further improve the heavy noble gas analyses was to build a new instrument with multiple multipliers and a zoom lens to allow simultaneous measurement of Kr and Xe. This has been achieved with custom built Noblesse from Nu-Instruments equipped with 8 miniature continuous dynode multipliers (channeltrons) from Burle (now Photonis). The other problem with the SuperGnome comes from the very property that makes it excel as a Xe/Kr instrument. The low extraction gradient, responsible for its excellent ion optics, is easily distorted by large ion densities (space-charge effect), and the high concentrations of SW hydrogen did just that.

Although the Noblesse was designed two decades after the SuperGnome, it could not approach the nearly 100% ion transmission of the SuperGnome. The Noblesse "Bright" ion source has only 65% transmission, implying that one of every three ions is wasted. In addition to not being counted, these ions are implanted into defining slits increasing "memory" effects. Another disadvantage of No-blesse is a relatively low counting efficiency of continuous dynode multipliers (~85%) and the "cross-talk" between adjacent multipliers (reaching up to 0.3%) caused both by proximity and poor shielding. Memory effects are minimized by the small difference between isotopic compositions of the SW and our standard, the terrestrial atmosphere. Channeltrons employed in our 8-multiplier Noblesse are neither very efficient nor very stable, but they were the only option at the time when Noblesse was designed. All that said, Noblesse with all its faults, is, as a multicollector instrument, effectively more sensitive than SuperGnome, and its zoom lens allows all Kr and Xe isotopes to be simultaneously analyzed, an impossible feat in any other instrument, including new Helix-MC^+ from ThermoFisher recently added to our facilities. For the low-abundant SW Kr and Xe where counting statistics are the dominant source of errors, the sensitive (1.8×10^{-16} cm^3 STP ^{132}Xe/cps) 8-multiplier Noblesse is the most suitable for measuring the heavy SW noble gases. Table 1 shows the arrangement of multipliers for the isotopic analyses of the heavy noble gases and illustrates the technique of internal calibration of the multipliers' efficiencies.

The reliability of our 8-multiplier Noblesse mass-spectrometer for analyses of small amounts of heavy noble gases has been demonstrated using multiple measurements of atmospheric noble gases corresponding to ~760,000 atoms of ^{132}Xe. The absolute Xe sensitivity (1.8 mA/Torr) varied less than 1.6% during the day (Hohenberg et al., 2005). The second Noblesse instrument with similar detector array in addition to air standards has been tested using small (few to few hundred μg) samples of Murchison meteorite, and it was found that after "burn-in" period the channeltrons remained fairly stable allowing reproducibility of major Xe isotope ratios of few & (Ott, 2010). Therefore we found unnecessary to analyze any additional standards. As it is discussed later we intended to avoid any noble gas samples which are isotopically and elementally different from atmospheric and SW compositions.

The absolute calibration of the atmospheric standard was made using our SuperGnome mass-spectrometer and the international Ar standard – biotite LP-6 (Charbit et al., 1998). The calibration of *the same* atmospheric standard (bottle and pipette) was independently carried out in the ETH lab by Veronica Heber who found 1.5% more ^{40}Ar than we did using

LP-6 standard. Taking the average of these two independent calibrations we calculated the amounts of Kr and Xe in one “pipette” and these values were used during this work.

2.2. Extraction of noble gases from Genesis solar wind collectors

There are several ways of extracting noble gases from different host materials. The first is simple pyrolysis, melting of the material carrying the SW and extracting noble gases in a single step from the melt. The second is step-wise pyrolysis – increasing the temperature incrementally in steps. This allows extraction by enhanced diffusion, first from the weakly bound sites, usually the shallowly implanted noble gas atoms (and most of the superficial contamination), then progressively from the more deeply implanted atoms. This method was extensively used in the analyses of SW implanted into lunar soils and breccias, SW-rich (referred to as gas-rich) meteorites and the Apollo SWC-experiments (Cerutti, 1974), and it is routinely employed in I–Xe dating (Hohenberg and Pravdivtseva, 2008) to separate hosts with different noble gas mobilities. The third technique, CSSE (Wieler et al., 1991), in contrast with step-wise pyrolysis, is a step-wise etching method. This is carried out at constant temperature, allowing a better depth resolution of SW noble gases and eliminating some of the mass-fractionation caused by diffusion in step-wise pyrolysis. An elegant version of CSSE was developed for Genesis gold SW-collectors which were step-wise amalgamated *in vacuo* by mercury vapor, thus incrementally releasing SW gases (Pepin et al., 2012). However, due to the relatively high procedural blanks for all of the above methods, none were suitable for the extraction of the low abundance heavy SW noble gases from Genesis collectors. Only laser ablation has the ability to delineate and selectively degas sub-micron surface layers carrying the implanted SW gases.

During Genesis noble gas analyses, the laser extraction techniques constantly evolved. Gradually increasing the applied UV-laser power with each raster was thought to be capable of separating surface contamination from the more deeply implanted SW noble gases. However, there were complications, especially for Kr and Xe, which needed several square centimeters of the PAC (Polished Aluminum Collector) material for the required isotopic precision. During the extraction process, ablated aluminum from the collector was deposited both on the walls of the extraction cell and on the internal surface of the vacuum viewport. This attenuated the laser power delivered to the sample and it heated the viewport and the whole extraction cell, increasing the blank and altering the power delivery to the surface, a critical part of our depth resolution. During the course and evolution of these analyses, several improvements (Fig. 1) were made which reduced the deposition of collector material on the viewport and associated viewport heating, reducing the background. All of these improvements have one thing in common: the SW-collector is tilted to the incident laser beam. Since there is no momentum transfer in laser ablation, the angular distribution of sputtered material flux is highly weighted in the direction perpendicular to the collector surface (e.g. Bennett et al., 1995). By allowing the laser to pass through the viewport and hit the surface at an oblique angle, the sputtered aluminum largely ends up on other parts of the extraction cell, harmlessly away from the vacuum viewport, shown in the Fig. 1. One drawback of this modification was a slight decrease in the depth resolution, but this is not a problem for the heavy noble gases which are removed in one-step ablation.

2.3. Purification of noble gases prior to isotope analysis

Although all of the Genesis collectors are made of ultra-pure materials in controlled environments, some terrestrial heavy noble gases can be trapped at the interface between the sapphire substrate and the deposited collector films. Interface contamination can be avoided by UV-laser depth control so that the extracted material does not extend down to the interface. Reduction of terrestrial contamination from material acquired during the hard landing was done by careful cleaning of the PAC surface to remove as much of this material as possible (Allton et al., 2006; Calaway et al., 2007). However, considering the fragility of the Al films on the AloS (Aluminum on Sapphire), these SW-collectors were not extensively cleaned. The only surface treatment of the AloS was the mechanical removal of suspicious dust particles and water spots and repeated rinses with acetone. Ultrasonic cleaning was not used since the mechanical stress can damage the Al films.

Contamination was not a problem for the analyses of the abundant light noble gases, but for the less abundant heavy gases variable contamination resulted in backgrounds well above the blank levels observed in the same material not flown on the mission. One explanation for the elevated and non-reproducible behavior of the heavy noble gas background was the notorious “brown stain”, a thin Si-based polymerized coating, observed on many flown collectors and on other surfaces of the spacecraft. Ozone plasma treatments reduced Xe and Kr blank to some extent, but the “flown” and “not-flown” AloS collectors still had very different Kr and Xe backgrounds. It was finally realized that neither contamination caused by the “hard” landing of the Genesis return capsule nor by the “brown stain”, could be responsible for the differences between the noble gas backgrounds of flight and the non-flight AloS collectors. Rather, it was the SW-hydrogen, the dominant SW component, present in quantities that cannot be effectively handled by conventional gettering, that makes the major difference between flight and non-flight material. The huge amounts of SW hydrogen, released during the Al-ablation of the SW-collectors, reacted with the surfaces of the vacuum system and the getter alloy itself. Surface oxide removal and reduction of reacted getter alloy liberates measurable quantities of noble gases which would otherwise remain trapped there. This effect is especially pronounced in getter alloys sintered in inert atmosphere enriched in noble gases. Elevated blank of all noble gases including helium was observed in vacuum systems contained the latest generation of SEAS getter alloys (Whitby, 2006). This effect is less pronounced in older generations of getters, like SAES NP-10, making them popular among noble gas community and manufacturers of noble gas mass spectrometers. Ultrahigh vacuum systems are known to be efficiently cleaned with hydrogen, and the liberated Kr and Xe from this inadvertent cleaning cause an enhanced blank. Therefore, the large quantities of SW hydrogen implanted and laser released from the collector must be quickly removed from the vacuum system to prevent noble gas contamination by such surface “cleaning”. To remove this hydrogen from vacuum system, we used a hot Pd-finger, a 5 mm diameter palladium tube with 0.3 mm walls, with the interior exposed to the extraction system and the exterior exposed to the atmosphere. When the Pd tube is heated to 500 °C, it removes 99% of hydrogen from the system to the atmosphere in less than 1 min, effectively solving our problem. It is essential that oxygen at atmospheric pressure be present on the exterior of the tube to remove the hydrogen by converting it to H_2O. Similar Pd-filters were employed in commercial mass-spectrometer

MI-9301 (Anufriev et al., 2006). They dramatically reduced hydrogen and protonated ions from the mass-spectra. The heated Pd-finger is main modification of our noble gas purification line which otherwise is similar to those used in conventional noble gas mass spectrometry.

3. RESULTS

3.1. Argon

Solar wind Ar has been analyzed in several different Genesis collectors by three different laboratories, and the measured SW $^{36}Ar/^{38}Ar$ ratios are all in a good agreement. Ratios listed in Table 2 were calculated under the assumption that the atmospheric $^{36}Ar/^{38}Ar$ = 5.305 (Lee et al., 2006). Interestingly, Genesis SW-Ar analyses agree better among themselves than the measurements of atmospheric $^{36}Ar/^{38}Ar$ (Mark et al., 2011 and Refs. therein).

In this work we carried out additional Ar measurements as a first step toward the more challenging measurements of SW-Kr and Xe. It was necessary to test our evolving UV-laser extraction techniques and to verify the performance of the modified multi-collector mass-spectrometer, both of which were never previously used in our laboratory for real measurements. Additionally, we attempted to analyze SW-Ar as a function of implantation depth by incrementally increasing UV-power delivered to the surface of PAC, which was chosen as the most abundant and readily available of the Genesis SW-collectors.

Short wavelengths for the extraction laser are needed to effectively couple with the highly polished surfaces of PACs, and short pulses are required to explosively excavate the material without heating it so we can achieve “clean” layer-by-layer extractions. For the latter, the pulse length must be short compared with thermal conduction time out of the laser pit. Our 266 nm quadrupled 30 Hz Q-switched NdYAG couples well and it produces a 5 ns long pulse, sufficient for the extraction requirements. The surface ablation of PAC was done in 23 steps by incrementally increasing UV-power from 0.3 to 6.2 mJ/pulse (corresponding to power densities from ~3 to 55 J/cm^2), with several steps being done at the same power (Table 3). Each subsequent raster covered a slightly smaller area to avoid degrading the depth resolution due to small but sometimes noticeable irreproducibility of the X–Y stage position, allowing edge material to be extracted. Surface concentrations of the released Ar shown in Table 3 are, therefore, normalized for each extraction step to account for the decreasing extraction areas. Another cause of degradation of the depth resolution is variable speeds of the X–Y stage. When the stage makes a U-turn, it slows down, momentary stops and then accelerates until it reaches the required speed in the opposite direction. Keeping the laser shooting during this maneuver can effectively “dig a trench” along two the sides of the ablation area. Therefore, a fast acting shutter was installed in order to redirect the laser beam from the moving extraction cell until the required speed of the stage is reached. The time lag of the shutter, runway time and all motions of the X–Y stage were controlled by LabView code via a GPIB interface.

An example of multi-collection of Ar isotopes is shown in Fig. 2. The arrangement of ion detectors for Ar analysis (Table 1) does not require changing of the magnetic field at all

providing the best possible counting statistics. To calculate the solar wind $^{36}Ar/^{38}Ar$ ratios, we know that the $^{40}Ar/^{36}Ar$ in the SW is small (an upper limit of 4.6×10^{-4} has been suggested from analyses of urelites by Göbel et al., 1978), suggesting that all of the ^{40}Ar is from terrestrial contamination and we assume that it is not significantly isotopically fractionated. There is no simple way to verify this assumption but Ar blanks are always of atmospheric composition and, since the ^{40}Ar is small anyway, this assumption is not very important for the corrections. Resulting $^{36}Ar/^{38}Ar$ ratios, corrected for atmospheric contamination, are shown in Table 3 and plotted in Fig. 3. The power step of 4.2 mJ/pulse has a measured $^{40}Ar/^{36}Ar$ ratio of 1.12 ± 0.01, among the lowest of all Genesis Ar measurements made so far, and demonstrates the negligible contribution from atmospheric Ar.

Visual observation of the UV-rastered area and repeated rastering at the same power (Table 3) suggest that the experimental setup was not optimal for “clean ablation”. Instead of a flat bottom for the laser excavated area, we observed a rough surface formed by molten Al that was not sputtered out of each laser pit, an observation confirmed by ZIGO interferometry (Butterworth, 2003). This “debris” in the excavated area will also couple to the laser and attenuate the laser power reaching the virgin surface, making complete Ar degasing from discrete layers in the PAC difficult at the ~7 mJ maximum power available in our experiment. Therefore, after completion of the laser ablation, the PAC was removed from the cell, the middle fragment of rastered area cut off, and it was placed in our small high vacuum extraction oven. After one month of degassing at 80 °C to remove superficial atmospheric Ar trapped by the fresh surface, it was melted to extract any remaining SW-Ar. About 4% of total SW-^{36}Ar was found in the pyrolysis step (Table 3), with its $^{36}Ar/^{38}Ar \sim 4.7$ being among the lowest observed in the entire experiment. This, however, does not appreciably affect reported results. It was done primarily for diagnostic reasons.

The calculated bulk SW-$^{36}Ar/^{38}Ar = 5.498 \pm 0.011$ (bottom of Table 2) is in good agreement with earlier analyses, which were done on a single multiplier instruments, bringing new confidence to our multi-collector mass-spectrometry intended to be primarily used for analyses of SW Kr and Xe. This result also allows us to slightly adjust the current best value for SW Ar: $^{36}Ar/^{38}Ar = 5.5005 \pm 0.0040$ (1σ).

Depth-dependent isotopic fractionation, a feature of constant velocity implantation, is now confirmed for Ar and in agreement with SRIM simulations. As can be seen in Table 3 and Fig. 3, the isotopic composition of SW-Ar becomes heavier with implantation depth. This effect, not appreciated until recently, could be partially responsible for the large variations in SW-$^{36}Ar/^{38}Ar$ measured in lunar regolith and in SW-rich meteorites (gas-rich meteorites) prior to the Genesis Mission. Depth-dependent fractionation, together with surface sputtering and diffusive losses, may well contribute to the range of $^{36}Ar/^{38}Ar$ values observed. The effect is even more important for Ne, being overlooked it led to an incorrect conclusion of the need for an addition heavy solar wind component (SEP Ne) to explain the range of Ne compositions observed in lunar material, and it is also applicable to Kr and Xe, which will be discussed in 4.2.

3.2. Krypton and Xenon

Argon extracted from the Genesis collectors contains some terrestrial contributions but, since the solar wind has negligible ^{40}Ar and the terrestrial isotopic ratios are known, this can easily be removed, leaving pure solar wind argon. For krypton and xenon, which are far less abundant in the solar wind, the terrestrial contamination becomes a serious problem and there is no “terrestrial only” isotope to identify that component. In fact, the compositions of SW and terrestrial noble gases are close, so accurate partitioning by isotopic composition is not possible. Our original intention was to use stepped-power laser extraction (described in 3.1.) to separate any superficial surface-correlated contamination from the more deeply implanted SW noble gases. A complicating factor here is the low abundances of the heavy noble gases in the SW, which requires analyzing very large areas of the collectors for precise measurements in stepped-power laser extractions. The conventional way to document terrestrial Xe and Kr contributions is to analyze reference (non-flight) SW collectors, manufactured in the same way as the flight collectors, utilizing the same procedures and the same raster areas. The Xe and Kr signals measured in these non-flight coupons would then be a proxy for the blanks of the actual collectors. Unfortunately, the AloS collectors were manufactured in several batches and, after the “hard” landing of the Genesis return capsule, it became challenging to pair flight and non-flight AloS material. That said, a more severe problem was found. In the laser extraction experiments it was observed that the Xe and Kr blanks were neither proportional to the raster areas, nor were they very reproducible. As discussed above, large quantities of implanted SW hydrogen released from SW collectors reacted with the getter material. Since the SAES getters were produced by sintering in an inert atmosphere, this liberated dormant Xe and Kr from the getter alloy. Removing hydrogen from the sample system using palladium (described in 2.3.) significantly reduced this problem, but did not eliminate it completely, so new techniques for minimizing terrestrial noble gases had to be developed.

An alternative approach for blank correction is based on the significant difference in the $^{84}Kr/^{132}Xe$ ratios between the terrestrial atmosphere and the solar wind. In the case of binary mixtures of SW and terrestrial components, the $^{84}Kr/^{132}Xe$ can be used as a measure of terrestrial contribution. It was critically important that our extraction and purification system as well as the multi-collector mass-spectrometer have seen *only* terrestrial and solar noble gases so that we can be limited to these two compositions (with negligible mass fractionation). The capability of simultaneously measuring both heavy noble gases in a single run is needed for this to work, but this was the plan all along (Table 1). This approach is described in Section 3.2.3.

The depth profile of SW-Ar observed in Fig. 3 suggests that an incomplete laser extraction of SW-Xe and SW-Kr may and will result in some fractionation, the preferential release of the lighter isotopes. Therefore, instead of one single step laser ablation, we employed three UV-power steps: The first one, ~1 mJ/pulse, to degas the very surface of the SW-collector, the second, full power of ~6.5 mJ/pulse (~58 J/cm^2), to extract essentially all gases in a single step, and the third, again with the full power, to verify the completeness of the extraction. Surprisingly the third step contained negligible amounts (≤2%) of SW gases, much less than in the case of a number of steps with incrementally increased laser power

settings, suggesting an inward diffusion of implanted SW caused by the heating at the intermediate power steps, and good news for the heavy noble gas analyses with fewer steps.

3.2.1. Krypton measurements—All potential sources of hydrocarbons were eliminated by using oil-free machining (only Anchorlube, a water soluble lubricant, was used in machining), electro-polishing (whenever possible) of vacuum components and replacing the original Edwards turbo-molecular pump, which contained a ~10 ml oil cartridge on the low-vacuum side, with an Osaka pump with a magnetically levitated rotor. However, we still had a problem associated with hydrocarbon interference at m/e = 78 due to the omnipresent C_6H_6 (benzene) which is not completely resolved from ^{78}Kr. Attempts to correct for benzene using hydrocarbons at m/e = 79 and 77, which were measured anyway (Table 1), were not successful. Luckily, ^{78}Kr, the lightest stable Kr isotope, passes through the outermost edge of the zoom lens and, when the electrostatic fringe field of the zoom lens is intentionally distorted, we can measure ^{78}Kr slightly off-center, where the contribution of benzene is almost negligible (Fig. 4). This distortion does not affect the other Kr isotopes which pass through the middle part of the lens, but it does provide means for partially resolving the benzene interference and obtaining valid ^{78}Kr measurements.

The second problem in Kr analyses was caused by the “change-of-charge” effect that interferes with the measurement of ^{80}Kr. In addition to the well-known doubly charged $^{40}Ar^{++}$ interference with the singly charged $^{20}Ne^{+}$, there is another effect of doubly charged $^{40}Ar^{++}$ which interferes with $^{80}Kr^{+}$. A small fraction of doubly charged $^{40}Ar^{++}$ ions can pick up an electron from the source defining slits or from ion-atom collisions between ion-source and magnet, becoming singly charged $^{40}Ar^{+}$ but with the twice the energy, thus following the same trajectory as $^{80}Kr^{+}$. Thus it is called “change-of-charge” effect and is clearly detectible whenever Kr is measured in the presence of ^{40}Ar. To minimize the effect, Ar must be cryogenically separated from Kr although complete Ar removal cannot be achieved without losing a small fraction of the Kr and fractionating the rest. At a temperature of −125 °C ~3% of the original Ar is still present on our activated charcoal trap, so an additional measure is required to further reduce the “change-of-charge” effect on ^{80}Kr. This was done by reduction of the electron energy from 100 to 75 eV at the cost of ~10% sensitivity loss. Luckily, the solar wind contains very little, if any, ^{40}Ar so most “change-of-charge” problems occur during the calibration of the mass spectrometer. This, however, is important, especially for Noblesse, since each multiplier must be individually calibrated.

3.2.2. Xenon measurements—Besides the general problem caused by low abundance of SW–Xe, there is one isotopically specific problem, the interference of $^{131}Xe^{+}$ with $C_3F_5^+$, which cannot be fully resolved by Noblesse. This fluorocarbon, apparently coming from surface of the plastic bags which are currently used for packaging vacuum components, is poorly soluble in the traditional cleaning liquids: acetone, methanol and de-ionized water. It is therefore omnipresent at very low levels in almost every modern mass-spectrometer. To solve this problem we used two approaches.

First, an additional cleaning step was added to the sample purification line. This step consists of a W-filament at >1500 °C, which can crack polymolecules into simpler compounds, and a Ti-sublimation pump in a ~150 cm^3 SS304 housing, with the same W–Ti

evaporation process as described by Hohenberg, 1980. This combination reduces $C_3F_5^+$ peak by factor ~10. The rest is taken care off by shifting ^{131}Xe slightly off center where the fluorocarbon contribution is negligible (similar to ^{78}Kr procedure, Fig. 4). Since only the two odd isotopes ^{129}Xe and ^{131}Xe are measured at this setting of magnet field and zoom lens (B2, Z2 in Table 1), it is easy to adjust the lens field in such a way that the position of ^{129}Xe peak remains unaffected by the ^{131}Xe shift.

The Noblesse mass spectrometer has a counting half-life for Xe of ~17 min, reflecting its far from ideal ion transmission and making memory effects more pronounced than in our high transmission instruments. To minimize these effects and to correct for them, only small spikes of atmospheric Xe and Kr were ever admitted into this mass spectrometer for calibrations, and all vacuum extraction, purification and pumping systems were assembled from new parts, never exposed to isotopically anomalous noble gases. Whenever possible, these parts were internally electro-polished to minimize hydro- and fluro-carbon contaminations. Pumping lines were made as short as possible with no pipes being thinner than ¾″ in diameter for maximum conductance. Additionally, the high voltage power supply for the ion source was modified to be switched on simultaneously with the beginning of noble gas measurements, providing a more precise “time zero” so that the measured noble gases have not been yet altered by memory growth.

3.2.3. Correction for trapped Xe and Kr—A binary mixture between SW and single terrestrial trapped components is described by the following equations:

$$^{84}\mathrm{Kr}_{\mathrm{SW}} = {}^{84}\mathrm{Kr}_{\mathrm{M}} \times \left[\left(\frac{^{132}\mathrm{Xe}}{^{84}\mathrm{Kr}} \right)_{\mathrm{M}} - \left(\frac{^{132}\mathrm{Xe}}{^{84}\mathrm{Kr}} \right)_{\mathrm{T}} \right] / \left[\left(\frac{^{132}\mathrm{Xe}}{^{84}\mathrm{Kr}} \right)_{\mathrm{T}} - \left(\frac{^{132}\mathrm{Xe}}{^{84}\mathrm{Kr}} \right)_{\mathrm{SW}} \right] \quad (1)$$

$$^{132}\mathrm{Xe}_{\mathrm{SW}} = {}^{132}\mathrm{Xe}_{\mathrm{M}} \times \left[\left(\frac{^{84}\mathrm{Kr}}{^{132}\mathrm{Xe}} \right)_{\mathrm{M}} - \left(\frac{^{84}\mathrm{Kr}}{^{132}\mathrm{Xe}} \right)_{\mathrm{T}} \right] / \left[\left(\frac{^{84}\mathrm{Kr}}{^{132}\mathrm{Xc}} \right)_{\mathrm{T}} - \left(\frac{^{84}\mathrm{Kr}}{^{132}\mathrm{Xe}} \right)_{\mathrm{SW}} \right] \quad (2)$$

where SW refers to Solar Wind, M to Measured and T to Trapped/Terrestrial, and the three unknowns are $^{132}Xe_{SW}$, $^{84}Kr_{SW}$ and $(^{132}Xe/^{84}Kr)_T$, because the latter may not be trapped in atmospheric proportion due to the tendency of Xe to be “stickier” than Kr.

The ratio $^{84}Kr/^{132}Xe = 9.55 \pm 0.16$ (Meshik et al., 2009) was determined employing a set of Genesis samples different from those used in this work. At that time we suspected an unaccounted blank contribution and preferred a conservative estimation: $^{84}Kr/^{132}Xe \leq 9.71$. Later Heber et al. (2009) reported SW $^{84}Kr/^{132}Xe = 9.5 \pm 1.0$ and Vogel et al. (2011) suggested 9.9 ± 0.3. For this study we adopted the value of 9.55 because it was determined using the same type of SW collector material (aluminum) as in this study, and it was measured by the same Noblesse mass spectrometer. Thus, even if the 9.55 value includes an unaccounted systematical error it will be automatically canceled in the data treatment we use for derivation of the SW isotope ratios.

Both PAC and AloS collectors were analyzed in different laser cells (shown in Fig. 1) using pulsed laser extraction at two wavelengths: 266 nm for PAC and 1064 nm for AloS. 24 individual areas from AloS and PAC were laser-ablated. To determine the actual trapped $(^{84}Kr/^{132}Xe)_T$ we assumed that in all of these analyses this ratio was constant and, with 24 available measurements, the system of Eqs. (1) and (2) is over-determined. A multi-variance solution can be obtained from minimization of the standard deviations of the SW fluences $^{84}Kr_{SW}$ and $^{132}Xe_{SW}$ measured for each experimental setup. This procedure is illustrated in Fig. 5. As expected, in all experiments the best convergence of $^{132}Xe_{SW}$ and $^{84}Kr_{SW}$ is observed at $(^{132}Xe/^{84}Kr)_T$ higher than in the terrestrial atmosphere, as expected, with a weighted average of $(^{132}Xe/^{84}Kr)_T = 0.041$, representing the most probable ratio of the trapped gases. This is ~12% higher than the atmospheric value of 0.036, implying that the atmospheric isotopic compositions of trapped Xe and Kr are probably not significantly altered.

Then, for each experimental setup we calculate the error-weighted fitting line forced through the trapped component. The intersection of this line with the *Y*-axis at the SW Xe/Kr = 9.55 corresponds to the isotope ratio of the SW. The fitting procedure took into account statistical (1σ) errors for measured isotope ratios and 5–7% errors for Xe/Kr values based on reproducibility of this ratio observed in atmospheric standards, which is significantly higher than statistical errors. However, because of relatively small slope of the fitting lines, these seemingly large error bars contribute little to the final SW isotope ratios and easily accommodate potential errors of the end members.

All Xe and Kr measurements are tabulated in Tables 4 and 5 and plotted in Figs. 6 and 7. Average blanks (without laser) have very large error bars (some of them are not shown because they exceed the plot size), but they are generally scattered about trapped values. For Kr the trapped contribution varies from ~5% to 50% and from ~3% to 20% for Xe, reflecting a relatively higher abundance of atmospheric Kr. For almost all analyses, for both Xe and Kr, the fraction of trapped gas is relatively small.

The Y-intersection of straight lines drawn through the experimental points and trapped values provide solar wind isotope ratios. Interestingly, these intersections are often determined more accurately when contributions of trapped gases are relatively large, confirming that counting statistics is the major source of uncertainty. Tables 6 and 7 show the weighted averages of calculated solar wind isotope ratios taken in different experiments carried out several months apart and in different geometries of the extraction cells (Fig. 1). Yet, the observed variations are all within the statistical uncertainties and therefore we can calculate general weighted average for all of the experiments, shown in Tables 6 and 7 as “All data (fixed trapped comp.)”.

3.2.4. Comparison of isotopic compositions of heavy noble gases with published Genesis data and best current estimates—SW-Ar composition measured in PAC (3.1) is in good agreement with independent analyses of other Genesis SW-collectors (Table 2). This allows us to calculate the weighted average among the most accurate results and propose the current best estimate of $^{36}Ar/^{38}Ar = 5.5005 \pm 0.0040$ which is shown at the bottom of Table 2.

Except for the $^{86}Kr/^{84}Kr$ ratio (the most abundant isotopes) measured in Genesis Si and diamond SW-collectors at ETH, no other Kr isotope ratios have been published so this work represents the first full isotopic analysis of Genesis SW Kr. The ETH values $^{86}Kr/^{84}Kr$ = 0.302 ± 0.003 (Heber et al., 2009) and 0.303 ± 0.001 (Vogel et al., 2011), agree with our value of $^{86}Kr/^{84}Kr$ = 0.3012 ± 0.0004 (Table 6, this work). Since the latter number is more precise and since it is based upon five series of independent analyses, it has demonstrated reproducibility, we suggest that the numbers listed at the bottom of Table 6 be considered as current best estimate for Genesis Mission SW Kr.

In contrast to Kr, more published data are available for Genesis SW-Xe. Prior to our analyses, the SW $^{129}Xe/^{132}Xe$ ratios were reported by Heber et al., 2009; Vogel et al., 2011. Major SW Xe isotopes analyzed using RELAX technique were illustrated in Fig. 6 of Burnett (2011). Crowther and Gilmour (2012) reported all Xe isotopes in the solar wind, except ^{126}Xe because of interference with hydrocarbons which apparently can be ionized by the RELAX technique along with Xe isotopes. This problem has been addressed later (Crowther and Gilmour, 2013) at the cost of increasing error bars, especially for ^{126}Xe and ^{128}Xe. For example, the reported 1σ error for $^{128}Xe/^{132}Xe$ is ~8% (Crowther and Gilmour (2013) which is 30 times higher than in this work. All the above Xe analyses are shown at the bottom of Table 7, as well as the weighted average of all available data, which we propose to use as current best estimate of Genesis SW-Xe isotopic composition.

4. DISCUSSION

4.1. Solar wind flux of heavy noble gases

The term “SW-fluence” used here is the total number of SW ions/cm^2 collected by Genesis between November 30, 2001, and April 1, 2004 at the L1 point (Resenfeld et al., 2007). The Genesis Mission collected SW for ~2.3 years (7.368×10^7 s) and the SW flux is the average number of SW ions/cm^2/s during the collection period.

The polished Al-collector (PAC, this work) recorded an average SW ^{36}Ar flux of 366 ± 6 in reasonable agreement with 381 ± 22 in AloS (Meshik et al., 2007), 397 ± 11 in DOS and Si (Heber et al., 2009) and 358 ± 11 in Au (Pepin et al., 2012). Assuming the absence of potential systematical errors associated with possible Ar losses from PAC (Mabry, 2009), and backscatter corrections from gold (Pepin et al., 2012), the formal weighted average among all these fluxes is 371 ± 5 of $^{36}Ar/cm^2/s$. We suggest using this value as a best current estimate for the average SW-^{36}Ar flux observed by Genesis. Given this new measure of the ^{36}Ar flux and ^{20}Ne flux from Mabry et al. (2007) and Meshik et al. (2007), the SW $^{20}Ne/^{36}Ne$ becomes ~56.5, closer to 51.5 ± 0.5 (Pepin et al., 2012) than to 43.2 ± 0.4 (Heber et al., 2009). The value of SW $^{20}Ne/^{36}Ne$ remains one of the major interlaboratory disagreements for Genesis SW compositions.

SW-fluences of ^{84}Kr and ^{132}Xe obtained in this study and reported by Zürich (Heber et al., 2009; Vogel et al., 2011) and Manchester (Crowther and Gilmour, 2013) groups are plotted in Fig. 8. The slope of apparent linear correlation between ^{84}Kr and ^{132}Xe fluences measured in different experiments in the course of this work cannot be used for calculation of the $^{84}Xe/^{132}Xe$ ratio since for the blank subtraction (see Section 3.2.3), we have assumed

$(^{84}Kr/^{132}Xe)_{SW}$ = 9.55, and it would be circular logic to calculate the already assumed value.

The weighted averages of ^{84}Kr and ^{132}Xe fluences obtained in this work (1.08 ± .05) × 10^7 and (1.15 ± .04) × 10^6 atoms/cm^2 agree with results reported by Heber et al., 2009; Vogel et al., 2011 and Crowther and Gilmour, 2013 (Fig. 8). This agreement is remarkable considering different SW collector materials and completely different approaches in blank correction used by different groups: the Kr/Xe ratio in St. Louis, non-flight references in Zürich, and cumulative error functions and variable kernel density estimations in Manchester. The general weighted average fluences (plotted in Fig. 8) are (1.15 ± .04) × 10^7 $^{84}Kr/cm^2$ and (1.18 ± .05) × 10^6 $^{132}Xe/cm^2$. Therefore the corresponding SW-^{84}Kr and SW-^{132}Xe fluxes of 0.156 ± 0.005 and 0.0160 ± 0.0007 atoms/cm^2/s can be considered as best current estimates.

4.2. Comparison with solar wind Kr and Xe analyses of young lunar regolithic material

The top panel of Fig. 9 shows the permil differences in isotopic composition of SW-Kr inferred by the analysis of lunar regolithic material (Pepin et al., 1995) relative to SW-Kr measured in Genesis Al-collectors in this study. While there is no statistical difference between these compositions within the rather large uncertainties, a distinct (~2‰/amu) mass fractionation is suggested, favoring the heavy isotopes in the lunar-derived SW compositions. These differences can be explained by diffusion, impact surface erosion, or enhanced by sputtering from radiation-damaged surfaces, leading to enhancements of the heavy Kr isotopes in the remaining lunar surface material, amplifying the effect of the depth-dependent fractionation of constant velocity implantation (favoring the heavy isotopes, as demonstrated for Ar in Fig. 3). The importance of such losses is clearly shown in the Ne depth profiling results on the Genesis Bulk Metallic Glass (BMG; Grimberg et al., 2006) compared with Ne closed system etching data on regolith samples (e.g. Benkert et al., 1993). The early BMG releases all have $^{20}Ne/^{22}Ne$ well above the average value of about 13.8 (like $^{36}Ar/^{38}Ar$ in Fig. 3), whereas the earliest regolith Ne releases *start* at 13.8, indicated that the surfaces of the regolith samples have been lost. These differences have been interpreted by Wieler et al. (2007) as showing that the surfaces of regolith samples are in sputtering steady state; however, it is not clear that regolith samples have received sufficient solar wind fluence to be in the steady state regime. Alternatively, these differences could also be due to secular variations of the solar wind (Genesis measured the contemporary SW, while the lunar value is integrated over perhaps a million years). If this is the case we can now set an upper limit for such variations at 2‰/amu.

The current best estimate of the Genesis SW Xe composition (Table 7) agrees with SW Xe derived from measurements of the lunar regolith material (Fig. 9, bottom) within few permil/amu level, and no significant linear fractionation is evident between the two. For all Xe isotopes, except the lightest ^{124}Xe, the Genesis analyses are more precise than compositions derived from the lunar regolith data. This suggests that in order to best explore potential differences and/or secular variations in SW Xe composition we first have to improve the lunar regolith analyses to utilize fully the precision of the Genesis SW Xe measurements.

4.3. Genesis Solar Wind Xe and the terrestrial atmosphere

The isotopic composition of terrestrial Xe remains not fully understood. There is no solar system Xe component from which the terrestrial atmospheric Xe can be made or derived by simple processes such as mass fractionation or the addition of any known radiogenic or other components.

To explain the isotopic composition of terrestrial Xe Pepin and Phinney (unpublished manuscript, 1976), using multi-dimensional isotopic correlations of the known chondritic Xe database, constructed a hypothetical component: U–Xe (the letter U does not refer to uranium). This component is mathematically derived exclusively from terrestrial and meteoritic data with no explicit reference to SW–Xe (Pepin, 1992). The composition of U–Xe is known to resemble the regolith SW spectrum for all Xe isotopes except the two heaviest: ^{134}Xe and ^{136}Xe which are significantly depleted in U–Xe relative to the SW (Pepin, 2000). With our Genesis SW data a more precise comparison of the SW and U–Xe compositions is now possible.

For the relatively abundant Xe isotopes at masses 128–132, the U–Xe and Genesis SW $^{128, 129, 130, 131}$Xe/^{132}Xe ratios (fixed trapped component, Table 7) differ by an average of only 0.1‰; the largest deviation, at ^{130}Xe/^{132}Xe, is −2.8 ± 2.6‰. The ^{124}Xe/^{132}Xe and ^{126}Xe/^{132}Xe ratios (involving the two lightest and least abundant Xe isotopes) are nominally higher in Genesis SW but their uncertainties overlap the U–Xe ratios. Therefore, it is now clear that U–Xe does not just resemble SW Xe at these isotopes; it is, in fact, compositionally solar, to high precision for these isotopes (^{128}Xe–^{132}Xe), although the ~5% deficit of ^{134}Xe and ~9% deficit of ^{136}Xe in U–Xe relative to SW–Xe is observed. Thus, if a process capable of selective depletion of the primordial terrestrial atmosphere in just two heaviest Xe isotopes can be found, the composition of terrestrial Xe could be derived from the SW–Xe composition.

4.4. Composition of Xe and Kr in phase-Q

In contrast to U–Xe which was never reproducibly observed, Q-noble gases represent the underlying constituent in all primitive meteorites (Busemann et al., 2000). While the Sun represents the largest solar system noble gas reservoir, and defines the starting material for solar system evolution, phase-Q is the most important reservoir for the heavy noble gases in meteorites. Xe-Q and Kr-Q have their highest concentrations in carbonaceous chondrites. The carrier for the Q-gases, called Phase-Q, is a peculiar trapping site (apparently carbonaceous, possibly elemental C) which survives hydrochloric and hydrofluoric acid dissolution of primitive meteorites such that only ~0.5% of the starting material remains but >90% of the heavy Q-gases (Ott, 2002). A major constituent of this material is nanodiamond (typically ~1%), a little SiC (~6 ppm) and graphite (<1 ppm), with the numbers referring to Murchison (Amari et al., 1994). Further oxidizing treatment with chemicals such as perchloric acid dissolves less than ~0.04% more of the remaining material (Lewis et al., 1975), but *all* of the Q-gases are removed with this treatment. The noble gas concentrations in phase-Q, usually calculated as the difference between gas concentrations in non-oxidized and oxidized HF/HCl residues, cannot be accurately determined until pure phase-Q is separated. But even the lower limit suggests that phase-Q has by far the highest Xe and Kr

concentrations of any known natural material and is, most likely, a 2-D carbonaceous film rather than a normal mineral host phase.

Heavy Q-gases are often considered as isotopically fractionated solar SW gases (Ozima et al., 1998; Podosek, 2003). The possible association of Xe-Q with Xe-HL carried by meteoritical nanodiamond (Huss and Lewis, 1994) was noticed by Lavielle and Marti (1992), Marti and Mathew (1998), Busemann et al. (2000), Gilmour (2010) and recently Crowther and Gilmour (2013). Now high precision Genesis analyses of SW-Kr and SW-Xe allow us to delineate more of the detailed structure of the relationship between Q and the SW. We will consider all Xe and Kr isotopes except ^{129}Xe, part of which may be the product of *in situ* decay of now-extinct ^{129}I ($T_{½} = 17 \times 10^6$ years) in the host phase itself. Nor have we considered Ar which has only two SW isotopes, making it impossible to resolve multi-component mixtures.

The method we use here is “goodness of fit” optimization of variable contributions of error-weighted end-member mixtures for the best match to the target composition. In noble gas geo- and cosmo-chemistry this method was used to model mantle degassing (Pepin and Porcelli, 2006), relationship between terrestrial noble gas reservoirs (Boehnke and Caffee, 2011), and “planetary” noble gas components (Gilmour, 2010 and Crowther and Gilmour, 2013). We essentially repeat this approach using our current best estimate for SW-Xe and SW-Kr.

In addition to fractionated SW, which is obviously a major factor in the transformation of solar gases into Q-gases, we will optimize the contributions of Xe-HL and Kr-HL (Huss and Lewis, 1994), and SiC and graphite, carriers of Xe-S and Kr-S (using the average composition of the G-component from Ott, 2002). We therefore have to optimize three parameters: the degree of isotopic fractionation of the SW and fractions of HL and S included which provide the best fit to the Q gases.

We used the GRG2 code (Generalized Reduced Gradient nonlinear optimization) to find a minimum possible value of $\chi^2 = ({}^iR_M - {}^iR_Q)^2/{}^i\sigma^2$, where ${}^iR_M$ is the isotope ratio in our model mix, ${}^i\sigma$ is the statistical error of this ratio, and iR_Q is the corresponding isotope ratio in Q. The meaning of χ^2 is similar to “goodness of fit”, but it is slightly different from reduced χ^2 used to check the agreement between observed and expected distributions when uncertainties of the model are unknown. In our case χ^2 is the average difference between isotopic ratios of our mixture and Q measured on σ-scale. Therefore if $\chi^2 \sim 1$ our model agrees with Q within 1σ, $\chi^2 \gg 1$ indicates a mismatch between our model and Q compositions. When $\chi^2 \ll 1$ we cannot make any definite conclusion – the uncertainties of our model composition are too large and more experiments are needed to reduce these uncertainties.

To determine whether or not additional components are really needed, the code was run in three steps. First, only the degree of linear fractionation of pure SW is determined without any additional components. This produces a $\chi^2 = 10$ and 8.7 for Xe and Kr, respectively (Table 8), indicating that Q-Xe and Q-Kr cannot be a product of linear fractionation of SW. Before Genesis measurements the fractionated SW (from young lunar regolith, Pepin et al.,

1995) differed from Q by only 2.2σ for both Xe and Kr allowing Ozima et al. (1998) to conclude that they are related by some form of mass-dependent fractionation. Now this difference is 10σ and ~9σ, for Xe and Kr respectively, suggesting that simple mass-fractionation is not sufficient to make Q from SW.

We then added variable amounts of HL gases (from Huss and Lewis, 1994). Xe-HL and Kr-HL contributions required for the best match were 1.6% and 0.1%, respectively, and optimal mass fractionations become less steep (Table 8). This step dramatically improved the goodness of fit for Xe ($\chi^2 = 1.8$) and much less significantly for Kr ($\chi^2 = 8.7$).

Finally a third component was added to the mixture of fractionated SW and HL gases, Kr-S and Xe-S, and all three of the parameters were optimized. In contrast to the second optimization step, now we observe a large improvement for Kr ($\chi^2 = 0.7$) and a modest χ^2 decrease for Xe ($\chi^2 = 1.6$). Both Xe-Q and Kr-Q require small addition of HL and 11–16 times smaller contribution of S (Table 8) while fractionated SW remains the major constituent of the Q-gases. Degree of fractionation required for the best match of SW + HL + S to Q is 8.2‰/amu for Xe and only 6.3‰/amu for Kr, which is difficult to explain if this fractionation is governed by only a mass-dependent process.

Fig. 10 shows the best achievable agreement between average compositions of Q-gases (Busemann et al., 2000) and the modeled mixtures of fractionated SW with the required HL and S additions. This agreement does not depend upon the starting compositions, indicating that the minimum of χ^2 is unique and global. The required ratio of Xe-HL/Xe-S is ~16, for Kr-HL/Kr-S it is ~11. It is quite possible that these numbers may change as the precision and accuracy of SW analyses will be further improved.

During the optimization procedure we allowed both positive and negative contributions of HL and S components. Only in one case a negative contribution of Xe–S was required – when SW composition was assumed to be same as observed in young lunar regolith (Table 8). This probably led Gilmour (2010) to conclude the absence of S component in the Q-gases in spite of clear presence of Kr-S. However, as it was mentioned earlier, it is not possible to draw any conclusion when χ^2 is only 0.2 (Table 8). Lunar regolith data were not accurate enough to conclude on presence or absence Xe-S in Xe-Q. Utilizing all Xe and Kr isotopes more accurate Genesis data suggest that both HL and S gases are needed to be present in fractionated SW to produce the composition of Q.

4.4.1. Implications of heavy Q-gases being derived from the Solar Wind—Since the host phase of Q-gases has not been yet isolated in pure form, it is a possibility that presolar components we observe simply represent impurities in HCl/HF residue. However, the cleanest sample of phase Q separated from nanodiamond-free Saratov (L4) has Xe composition indistinguishable from the Busemann's Q-Xe (Amari and Matsuda, 2012). Therefore, it appears unlikely that the HL and S components are just impurities in the samples analyzed. This also suggests that presolar gases in phase Q may not be carried by nanodiamond and SiC, but rather by some not yet identified phase produced by destruction (radiation damage?) of the host grains. It could be a graphene-like material observed by Stroud et al. (2012).

Products of nucleosynthetic p-, r-, and s-processes in Q-gases apparently support presolar origin of phase Q (Huss and Alexander, 1987). In this model phase Q trapped noble gases in the molecular cloud from which the Sun was later formed. However considering the sign of isotopic fractionation, it is difficult to make solar gases from Q. It is also unlikely that presolar solids adsorbed high concentrations of Q-gases in molecular cloud where density was only 10^2–10^6 protons/cm^3.

More comforting is an alternative view which considers Q-gases being locally derived from an initial nebula mix, now represented by the Sun (Hohenberg et al., 2013). The solar nebula and proto-Sun coexisted with surviving presolar grains, including carriers of HL and S noble gases. At that time low energy ions could be acquired by the grains already containing presolar gases. Large surface concentrations of heavy noble gases may result from “anomalous” adsorption (chemical bonding) with fractionation similar to that in Q (Hohenberg et al., 2002). The recent finding of SW nitrogen (as measured by Genesis) in phase Q (Verchovsky et al., 2013) lends more support for this scenario.

5. CONCLUSION

We have determined the isotopic composition of all heavy noble gases in contemporary solar wind delivered by Genesis mission. For all but the least abundant Kr and Xe isotopes, the Genesis analyses are presently the most precise measurements of the solar wind. Our 8 multiplier Noblesse with electrostatic zoom lens remains the best available instrument for analyses of heavy noble gases in the solar wind. We plan to do more analyses of Genesis SW collectors as we continue to improve our techniques to further the precision for the heavy noble gases, particularly for lightest isotopes ^{124}Xe and ^{126}Xe. It is critically important to use the same pristine multi-collector mass spectrometer which has no isotopic memory from any anomalous samples, with the only materials analyzed being the terrestrial atmosphere and the solar wind.

Acknowledgments

We are grateful to Judy Allton, Patti Burkett, Wally Calaway, Amy Jurewicz, Karen McNamara, Melissa Rodriguez (Genesis Science team) and John Saxton and Phil Freedman (Nu Instruments) for their support. We thank Gregory Herzog, Kurt Marti, Robert Pepin and Jamie Gilmour for their valuable comments. This work is funded by NASA Grants NNX09AC57G and NNX13AD14G.

References

Allton, JH., Wentworth, SJ., Rodriguez, MC., Calaway, MJ. Lunar Planet Sci XXXVIII. Lunar Planet. Inst.; Houston: 2006. Cleaning Genesis solar wind collectors with ultrapure water: Residual contaminant particle analysis. #2138 (abstr.)

Amari, S., Matsuda, J. Lunar Planet Sci XXXXIII. Lunar Planet. Inst.; Houston: 2012. Noble gas study of Q-rich fractions from Saratov (L4). #1051 (abstr.)

Amari S, Lewis RS, Anders E. Interstellar grains in meteorites: I. Isolation of SiC, graphite, and diamond; size distributions of SiC and graphite. Geochim Cosmochim Acta. 1994; 58:459–470.

Anufriev GS, Boltenkov BS, Ryabinkov AI. High-resolution mass spectra of residual gas in a metallic vacuum system. Tech Phys. 2006; 51(1):100–111.

Basford, JR., Dragon, JC., Pepin, RO., Coscio, MR., Murthy, VR. Krypton and Xenon in lunar fines. Proc 4th Lunar Planet Sci Conf; Houston, TX. 1973. p. 1915-1955.

Becker, RH. Lunar Planet Sci XXIX. Lunar Planet. Inst.; Houston: 1998. Effect of grain-surface erosion of solar wind isotopic ratios and the SEP mixing in extraterrestrial samples. #1329 (abstr.)

Becker RH, Schlutter DJ, Rider PE, Pepin RO. An acid-etch study of the kapoeta achondrite: implication for the argon-36/argon-38 ratio in the solar wind. Meteorit Planet Sci. 1998; 33:109–113.

Benkert J-P, Baur H, Signer P, Wieler R. He, Ne, and Ar from solar wind and solar energetic particles in lunar ilmenites and pyroxenes. J Geophys Res. 1993; 98(E7):13147–13162.

Bennett TD, Grigoropoulos P, Krajnovich DJ. Near-threshold laser sputtering of gold. J Appl Phys. 1995; 77(2):849–864.

Boehnke, P., Caffee, MW. Lunar Planet Sci XXXXII. Lunar Planet. Inst.; Houston: 2011. Terrestrial xenon in noble gas reservoirs. #2336 (abstr.)

Burnett DS, Barraclough BL, Bennett R, et al. The Genesis discovery mission: return of solar matter to earth. Space Sci Rev. 2003; 105:509–534.

Burnett DS, Genesis Science Team. Solar composition from the Genesis Discovery Mission. PNAS. 2011 Nov 29; 108(48):19147–19151. [PubMed: 21555545]

Busemann H, Baur H, Wieler R. Primordial noble gases in phase Q in carbonaceous and ordinary chondrites studied by closed-system stepped etching. Meteorit Planet Sci. 2000; 33:949–973.

Butterworth AL. Personal communication. 2003

Calaway, MJ., Burnett, DS., Rodriguez, MC., Sestak, S., Allton, JH., Stansbery, K. Lunar Planet Sci XXXVIII. Lunar Planet. Inst.; Houston: 2007. Decontamination of Genesis Array materials by ozone cleaning. #1627 (abstr.)

Cerutti, H. PhD thesis. University of Bern; 1974. Die Bestimmung des Argons im Sonnenwind aus Messungen an den Apollo-SWC-Folien.

Charbit S, Guillou H, Turpin L. Cross calibration of K-Ar standard minerals using an unspiked Ar measurement technique. Chem Geol. 1998; 150:147–159.

Crowther SA, Gilmour JD. Measuring the elemental abundance and isotopic signature of solar wind xenon collected by Genesis mission. J Anal At Spectrom. 2012; 27:256–269.

Crowther SA, Gilmour JD. The Genesis solar wind composition and its relationship to planetary xenon signatures. Geochim Cosmochim Acta. 2013; 123:17–34.

Heber VS, Wieler R, Baur H, Olinger C, Friedmann TA, Burnett DS. Noble gas composition of the solar wind as collected by the Genesis Mission. Geochim Cosmochim Acta. 2009; 73:7414–7432.

Hohenberg CM. High sensitivity pulse-counting mass spectrometer system for noble gas analysis. Rev Sci Instr. 1980; 51(8):1075–1082.

Hohenberg CM, Pravdivtseva OV. I-Xe dating: from adolescence to maturity. Chemie der Erde. 2008 Geochemistry;68:339–351.

Hohenberg CM, Thonnard N, Meshik A. Active capture and anomalous adsorption: new mechanisms for the incorporation of heavy noble gases. Meteorit Planet Sci. 2002; 37:257–267.

Hohenberg, CM., Marrocchi, Y., Meshik, AP., Mabry, JC., Saxton, JM., Freedman, P. AGU Fall Meeting. San Francisco: 2005. Noble gases in Genesis Collector material: New Measurement Capabilities. (invited talk). # SH32A-05 (abstr.)

Hohenberg CM, Meshik A, Pravdivtseva O. Xe-Q: From Here or There and How. 76th Annual Meeting of the Meteoritical Society. 2013 #527. (abstr.).

Huss GR, Alexander EC Jr. On the pre-solar origin of the normal planetary noble gas componernt in meteorites. Proc 17th Lunar Planet Sci Conf: J Geophys Res. 1987; 92:E710–E716.

Huss GR, Lewis RS. Noble gases in presolar diamond I: three distinct components and their implications for diamond origins. Meteoritics. 1994; 29:791–810.

Geiss J, Büchler F, Cerutt H, Eberhardt P, Filleux CH, Meiste J, Signer P. The Apollo SWC experiment: results, conclusions, consequences. Space Sci Rev. 2004; 110:307–335.

Göbel R, Ott U, Begemann F. On trapped noble gases in ureilites. J Geophys Res. 1978; 83:855–867.

Gilmour JD. Planetary noble gas components and nucleosynthetic history of solar system material. Geochim Cosmochim Acta. 2010; 74:380–393.

Grimberg A, Baur H, Bochsler P, Bühler F, Burnett DS, Hays CC, Heber VS, Jurewicz AJG, Wieler R. Solar wind neon from Genesis: implication for the lunar noble gas record. Science. 2006; 314:1133–1135. [PubMed: 17110575]

Grimberg A, Burnett DS, Bochsler P, Baur H, Wieler R. Compositionj of light solar wind noble gases in the bulk metallic glass flown on Genesis Mission. Space Sci Rev. 2007; 130:293–300.

Grimberg A, Baur H, Büchler F, Bochsler P, Wieler R. Solar wind helium, neon, and argon isotopic and elemental composition: data from the metallic glass flown on NASA's Genesis Mission. Geochim Cosmochim Acta. 2008; 72:626–645.

Jurewicz AJG, Burnett DS, Wiens RC, Friedmann TA, Hays CC, Hohlfelder RJ, Nishizumi K, Stone JA, Woolum DS, Becker R, Butterworth AL, Campbell AJ, Ebihara M, Franchi IA, Heber V, Hohenberg CM, Humayun M, McKeegan KD, Mcnamara K, Meshik A, Pepin RO, Schlutter D, Wieler R. The Genesis solar-wind collector materials. Space Sci Rev. 2003; 105:535–560.

Lee JY, Marti K, Severinghaus JP, Kawamura K, Yoo HS, Lee JB, Kim JS. A redetermination of the isotopic abundances of atmospheric Ar. Geochim Cosmochim Acta. 2006; 70:4507–4512.

Lewis RS, Srinivasan B, Anders E. Host phase of strange xenon component in Allende. Science. 1975; 190:1251–1262.

Lewis RS, Amari S, Anders E. Interstellar grains in meteorites: II. SiC and its noble gases. Geochim Cosmochim Acta. 1994; 58:471–494.

Lavielle B, Marti K. Trapped xenon in ordinary chondrites. J Geophys Res. 1992; 97:20,875–20,881.

Mabry, JC. Ph D thesis. Washington Univ; 2009. Solar Wind Helium, Neon, and Argon in Genesis Aluminum Collectors.

Mabry, JC., Meshik, AP., Hohenberg, CM., Marrocchi, Y., Pravdivtseva, OV., Wiens, RC., Olinger, C., Reisenfeld, DB., Allton, J., Bastien, R., McNamara, K., Stansbery, E., Burnett, DS. Lunar Planet Sci XXXVIII. Lunar Planet. Inst.; Houston: 2007. Refinement and implication of noble gas measurements from Genesis. #2412 (abstr.)

Marti K, Mathew KJ. Noble gas components in planetary atmospheres and interiors in relation to solar wind and meteorites. Earth Planet Sci. 1998; 107:425–431.

Mark DF, Stuart FM, de Podesta M. New high-precision measurements of the isotopic composition of atmospheric argon. Geochim Cosmochim Acta. 2011; 75:7494–7501.

Meshik A, Mabry J, Hohenberg C, Marrocchi Y, Pravdivtseva O, Burnett D, Olinger C, Wiens R, Reisenfeld D, Allton J, McNamara K, Stansbery E, Jurewicz AJG. Constraints on neon and argon isotopic fractionation in solar wind. Science. 2007; 318:433–435. [PubMed: 17947578]

Meshik, AP., Hohenberg, CM., Pravdivtseva, OV., Mabry, JC., Allton, JH., Burnett, DS. Lunar Planet Sci XXXX. Lunar Planet. Inst.; Houston: 2009. Relative Abundances of Heavy Noble Gases from the Polished Aluminum Solar Wind Collector on Genesis. #2037 (abstr.)

Meshik, A., Hohenberg, C., Pravdivtseva, O., Burnett, D. Lasar, M., editor. Measuring the isotopic composition of solar wind noble gases; Exploring the Solar Wind. 2012. p. 93-121.InTech(http://www.intechopen.com/books/exploring-the-solar-wind)

Porcelli, D.Ballentine, CJ., Wieler, R., editors. Noble gases in Geochemistry and Cosmochemistry. Mineralogical Society of America. USA: 2002.

Ott U. Noble Gases in Meteorites – Trapped Components. Reviews in Mineralogy and Geochemistry. 2002; 47:71–100.

Ott, U., Haubold, R., Hermann, S., Sudek, C. 73rd Meteoritical Society Meeting. New York: 2010. Urelite noble gases measured by multiple ion-counting mass spectrometry. # 5096 (abstr.)

Ozima, M., Podosek, F. Noble Gas Geochemistry. second. Cambridge University Press; 2002.

Ozima M, Wieler R, Marty B, Podosek FA. Comparative studies of solar, Q-gases and terrestrial noble gases, and implications on the evolution of the solar nebula. Geochim Cosmochim Acta. 1998; 62:301–314.

Palma RL, Becker RH, Pepin RO, Schlutter DJ. Irradiation records in regolith materials, II: Solar wind and solar energetic particle components in helium, neon, and argon extracted from single lunar mineral grains and from Kapoeta howardite by stepwise pulse heating. Geochim Cosmochim Acta. 2002; 66:2929–2958.

Pepin RO. Origin and noble gases in the terrestrial planets. Annu Rev Earth Planet Sci. 1992; 20:289–430.

Pepin RO. On the isotopic composition of primordial xenon in terrestrial planet atmospheres. Space Sci Rev. 2000; 92:371–395.

Pepin RO, Porcelli D. Xenon isotope systematics, giant impacts, and manle degassing on the early Earth. Earth Planet Sci Lett. 2006; 250:470–485.

Pepin RO, Becker RH, Rider PE. Xenon and Krypton in extraterrestrial regolith soil and in the solar wind. Geochim Cosmochim Acta. 1995; 59:4997–5022.

Pepin RO, Schlutter DJ, Becker RH, Reisenfeld DB. Helium, neon, and argon composition of the solar wind as recorded in gold and other Genesis collector materials. Geochim Cosmochim Acta. 2012; 89:62–80.

Podosek, FA. Treatise on Geochemistry. Vol. 1. Elsevier; 2003. Noble Gases; p. 381-405.Meteorites, Comets, and Planets

Resenfeld DB, Burnett DS, Becker RH, Grimberg AG, Heber VS, Hohenberg CM, Jurewicz AJG, Meshik A, Pepin RO, Raines JM, Schlutter DJ, Wieler R, Wiens RC, Zurbuchen TH. Elemental abundances of the bulk solar wind: analyses from Genesis and ACE. Space Sci Rev. 2007; 130:79–86.

Stroud RM, Chisholm MF, Amari S, Matsuda J. Aberration-corrected stem of Q-rich separates from the Saratov (L4) meteorite. 75th Meteoritical Society Meeting. 2012 #5229 (abstr.).

Tamhane AS, Agrawal JK. Diffusion of rare gases of solar wind origin from lunar fines as bubbles. Earth Planet Sci Lett. 1978; 42:243–250.

Verchovsky AB, Sephton MA, Wright IP. Isotopically light (Solar?) nitrogen associated with planetary noble gas carrier (Q). Coldschmidt 2013 Conference Abstracts 2406. 2013

Vogel N, Heber VS, Baur H, Burnett DS, Wieler R. Argon, krypton, and xenon in the bulk solar wind as collected by the Genesis Mission. Geochim Cosmochim Acta. 2011; 75:3057–3071.

Whitby J. Personal communication. 2006

Wieler R, Anders E, Baur H, Lewis RS, Signer P. Noble gases in phase Q: closed-system etching of an Allende residue. Geochim Cosmochim Acta. 1991; 55:1709–1722.

Wieler R, Grimberg A, Heber VS. Consequences of the non-existence of the SEPcomponent for noble gas geo-and cosmochemistry. Chem Geol. 2007; 244:382–390.

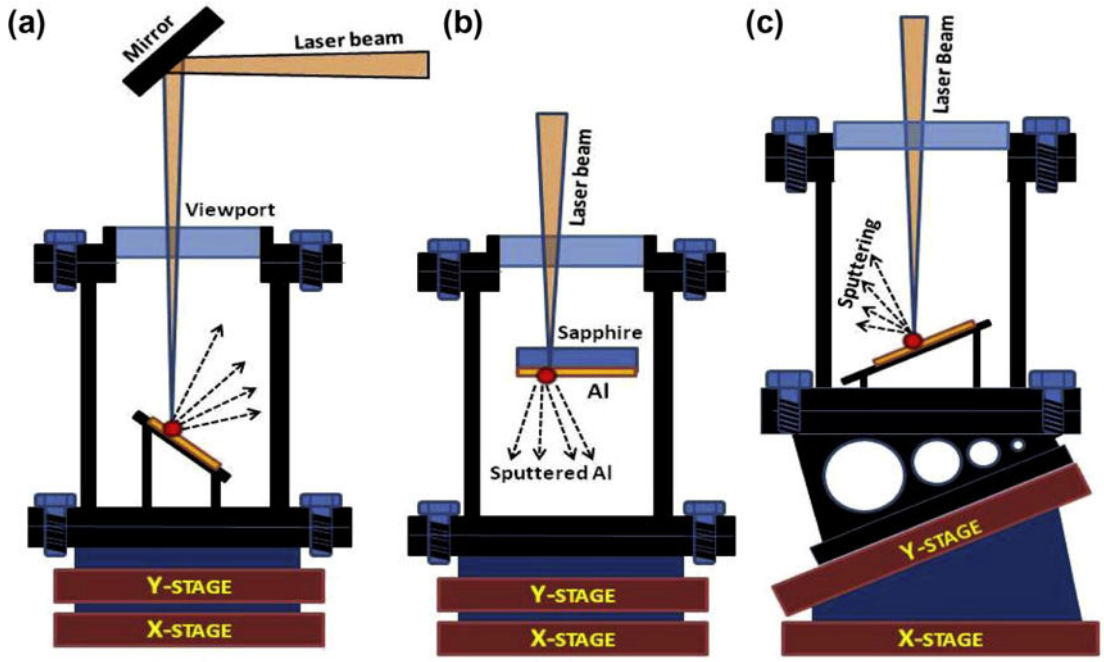

Fig. 1.

Three laser extraction cells used for laser extraction of SW noble gases from Genesis Al-collectors. The X-stage moves perpendicular to the figure plane, the Y-stage moves from left to right. The angle between the laser beam and the normal to the ablated surface is $\pi/4$ (a), π (b) and $\pi/8$ (c). The laser spot (~0.1 mm) remains in focus as the stages move. Long focal distances (250 mm (a) and 80 mm (c) provide "depth of field" sufficient to make variations of power density within the laser spot negligible. The cells (a) and (c) were used for ablation of both AloS and PAC, cell (b) is only suitable for SW collectors with transparent sapphire substrates, like AloS.

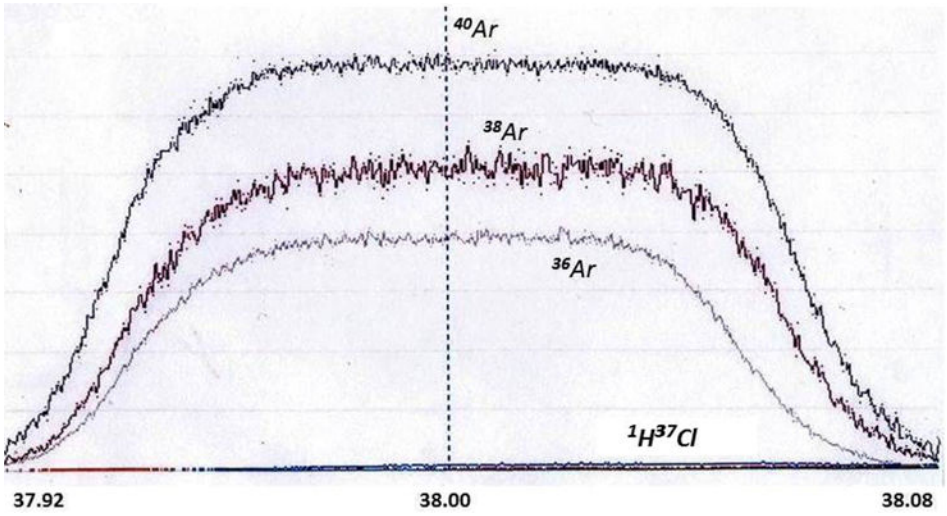

Fig. 2.

Multicollection of Ar isotopes directed to three different ion detectors according Table 1 (last line). Other detectors are used for ^{37}Cl needed for correction for HCl interferences, and baseline corrections. Therefore Ar measurements do not require changing magnet field. Horizontal axis is mass for central (axial) isotope ^{38}Ar.

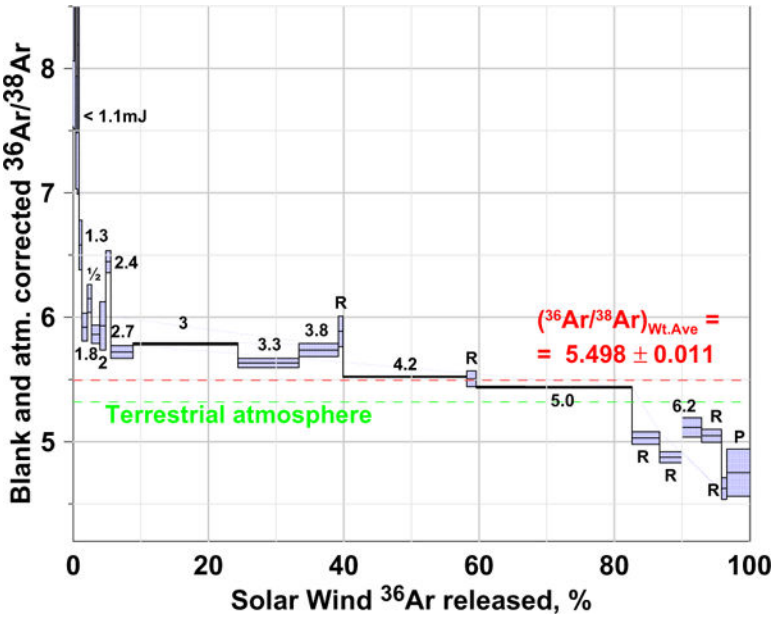

Fig. 3.

Depth profile of SW-Ar from Genesis PAC obtained using UV-laser ablation with incrementally increased power. Ar in each step has been corrected for the atmospheric contamination assuming that ^{40}Ar is absent in the SW. Numbers indicate laser output in mJ, R is re-raster with the same power, P stands for pyrolysis made after the completion of laser ablation. Dashed lines show sum of all steps (red) and terrestrial atmospheric Ar for the reference (green). Error bars are 1σ.

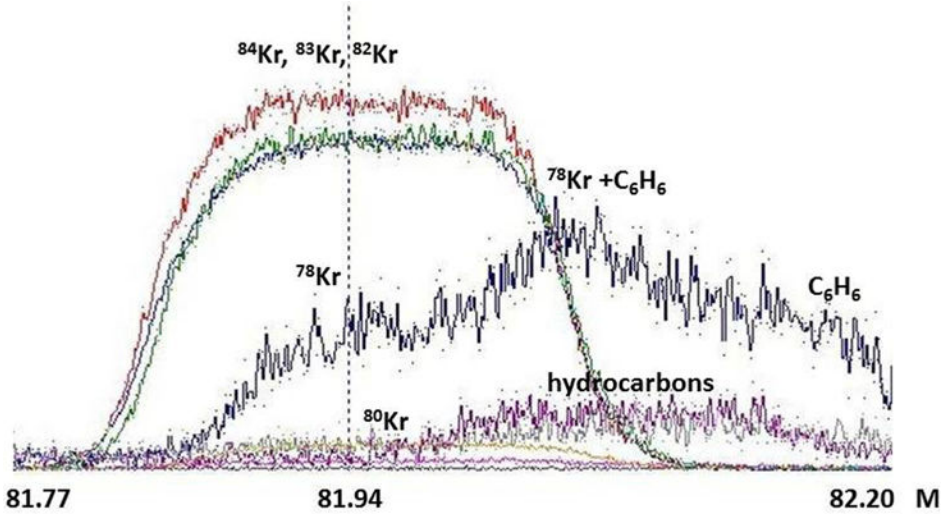

Fig. 4.

Simultaneous detection of Kr isotopes, except ^{86}Kr. Intentional fringe field distortion of the electrostatic zoom lens allows measurement of ^{78}Kr without significant benzene contribution. Vertical scales (count rates) are different for different isotopes. Horizontal axis is mass for central (axial) isotope – ^{82}Kr. The assignment of collectors corresponds to step 4 in Table 1.

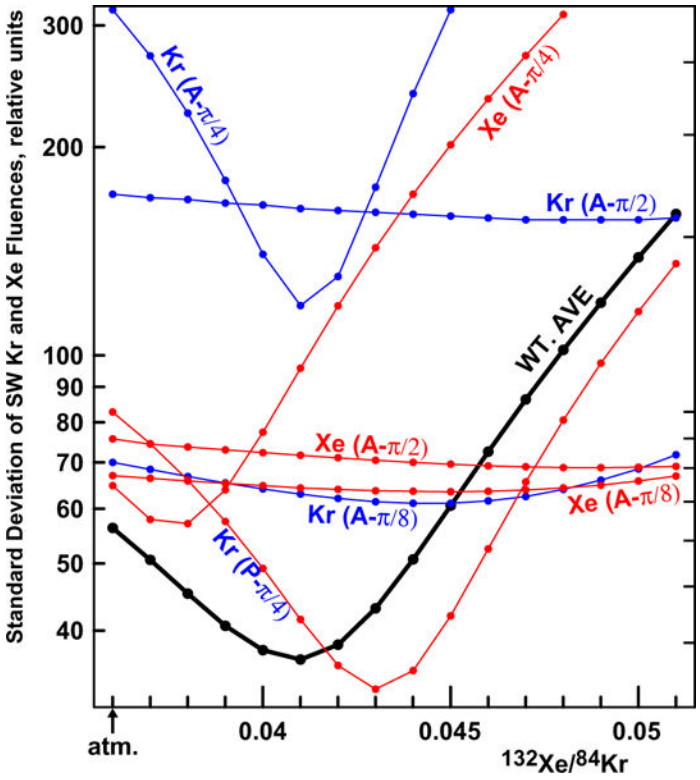

Fig. 5.

The convergence of SW-Xe and SW-Kr fluences at $^{132}Xe/^{84}Kr = 0.041$, which most probably represents the trapped terrestrial value of $^{132}Xe/^{84}Kr$.

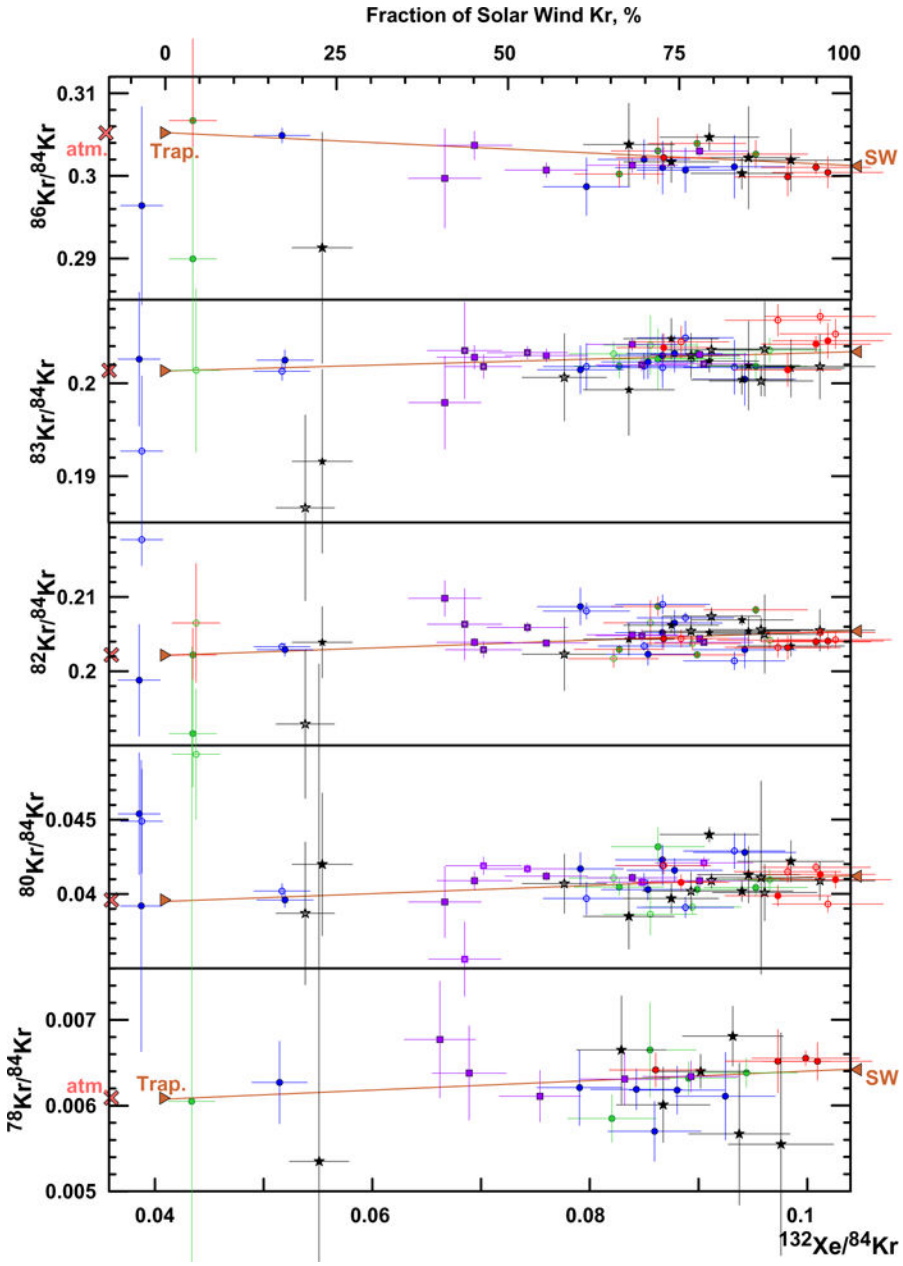

Fig. 6.

Kr isotopic composition measured in Genesis Al collectors. Fitting error-weighted lines are forced through the estimated trapped component. Inferred SW-Kr ratios are intercepts with right Y-axes at SW value of $^{132}Xe/^{84}Kr = 0.105$. Different colors correspond to different experimental conditions and within statistical errors result in the same SW composition. Errors are 1σ.

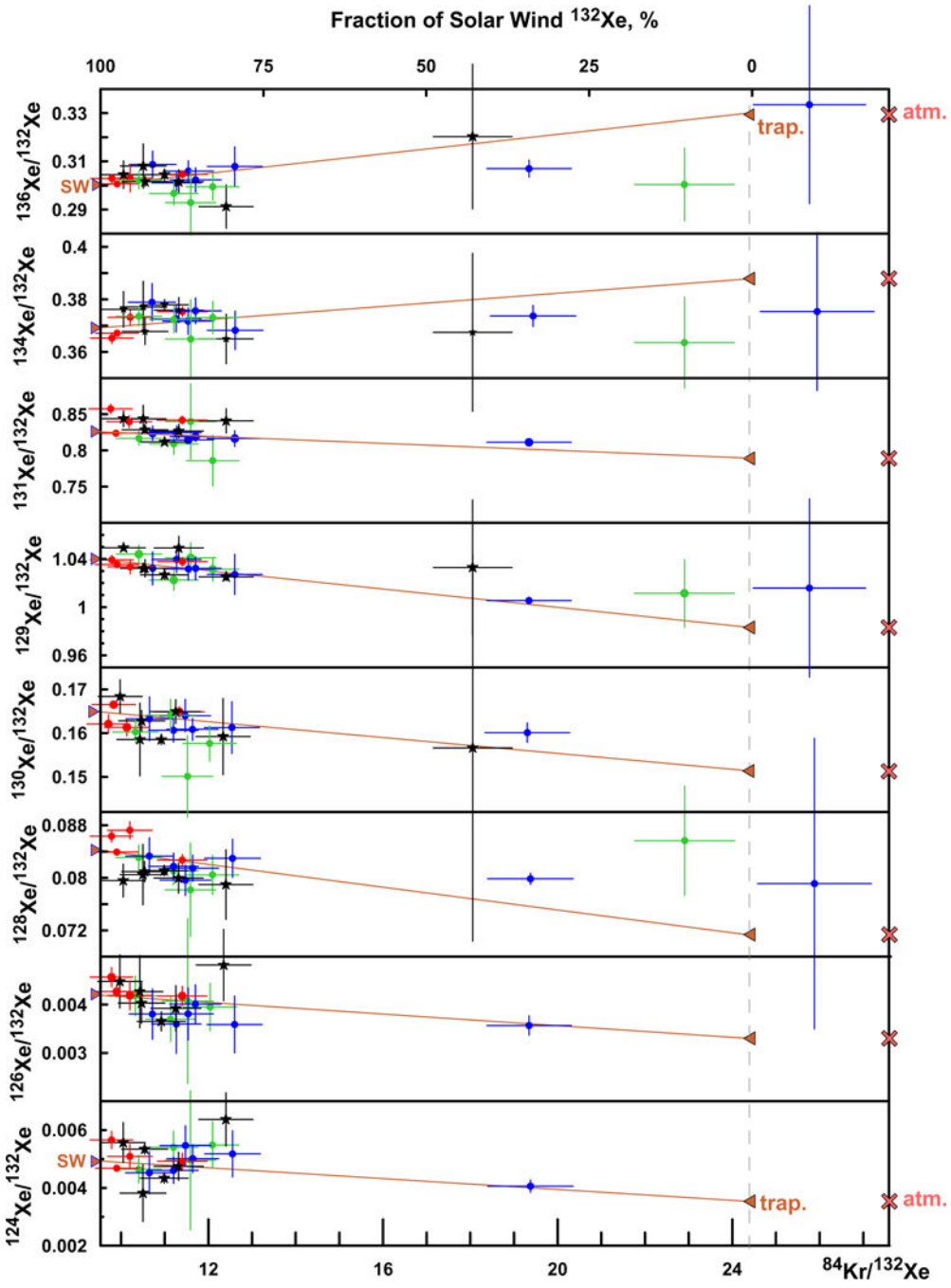

Fig. 7.

Xe isotopic composition in Genesis Aluminum collectors. Fitting error weighted lines are forced through the estimated trapped component. Inferred SW-Xe ratios are intercepts with left *Y*-axes at SW value of $^{84}Kr/^{132}Xe = 9.55$. Different colors correspond to different experimental conditions and within statistical errors give the same SW composition. Errors are 1σ.

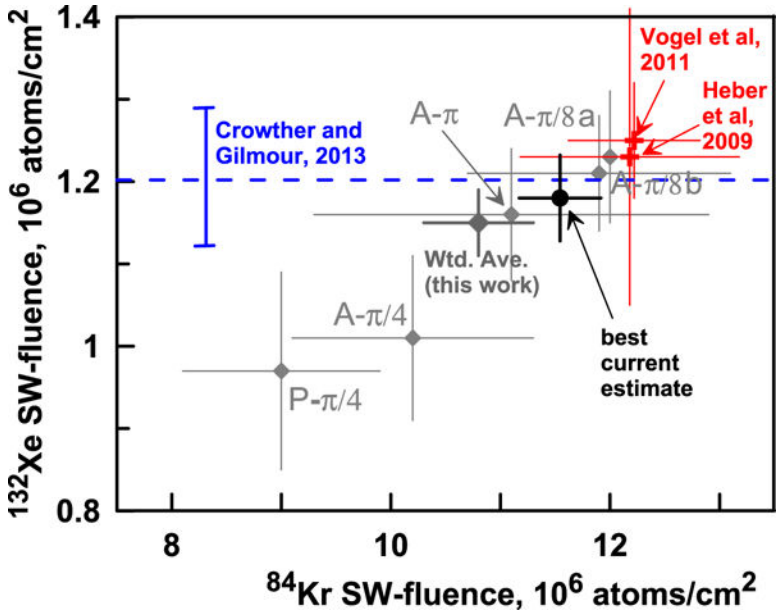

Fig. 8.

SW-fluences measured in different experiments in the course of this work (grey) and their weighted average $^{84}Kr = (1.08 \pm .05) \times 10^7$ at/cm^2 and $^{132}Xe = (1.15 \pm .04) \times 10^6$ at/cm^2 (black) are in reasonable agreement with independent analyses of different SW collectors.

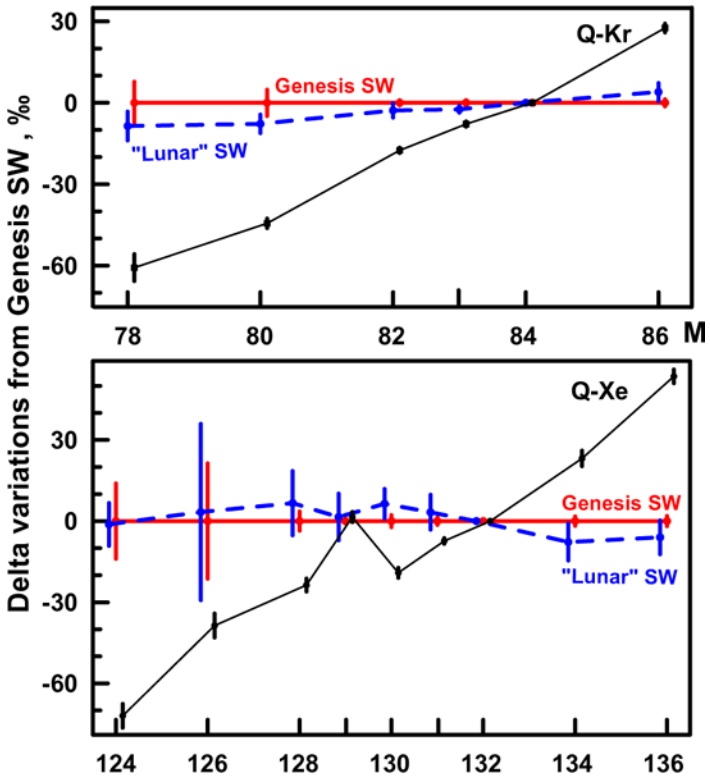

Fig. 9.

"Lunar" SW (blue, Pepin et al., 1995) and Q-gases (black, Busemann et al., 2000) *vs.* Genesis SW (red, this work). Although normalized to the Genesis composition as a delta plot, the errors shown (1σ) are not propagated, so overlapping error bars infer consistency.

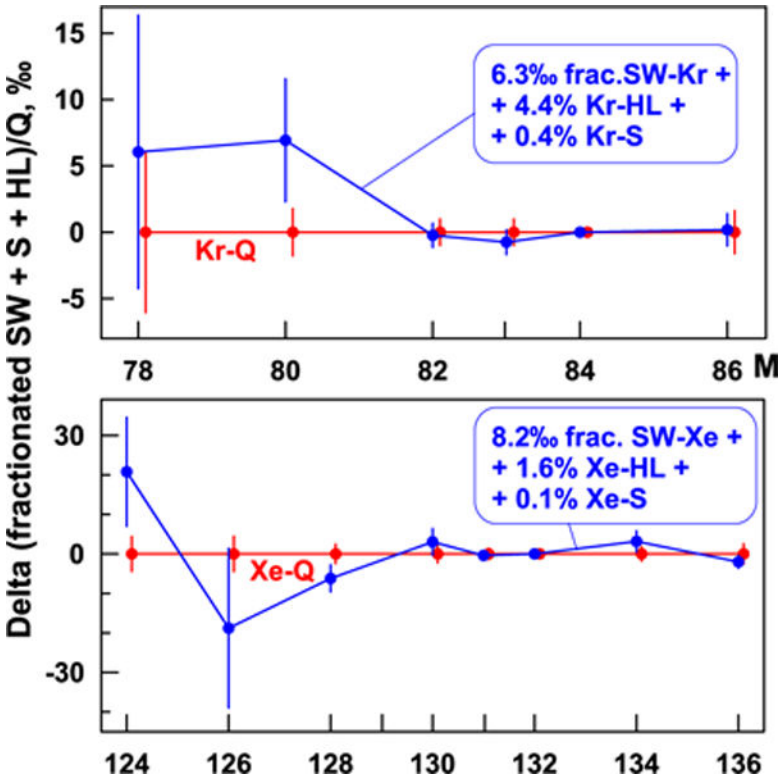

Fig. 10.

Model composition of Q-gases, based on the best current estimate of the Genesis SW composition (blue, this work), *vs.* Q-gases (red, Busemann et al., 2000). Errors (1σ) are not propagated to delta values.

Table 1

Assignment of ion collectors for isotope analyses of heavy noble gases. All Kr and Xe isotopes are measured simultaneously in only four steps of magnet field and zoom lens, with Kr being analyzed twice using adjacent detectors for internal calibration of counting efficiencies. No changing of magnetic field and zoom lens are needed for Ar analyses.

Magnet, Zoom lens settings	**Ion collectors (EM – electron multipliers, FC – Faraday Cup)**								
	FC	**EM1**	**EM2**	**EM3**	**EM4**	**EM5**	**EM6**	**EM7**	**EM8**
B1, Z1		^{136}Xe	^{134}Xe	^{132}Xe	^{130}Xe	^{128}Xe	^{126}Xe	^{124}Xe	
B2, Z2				^{131}Xe	^{129}Xe				
B3, Z3		^{86}Kr		^{84}Kr	^{83}Kr	^{82}Kr		^{80}Kr	
B4, Z4	^{86}Kr		^{84}Kr	^{83}Kr	^{82}Kr		^{80}Kr		^{78}Kr
B5, Z5	^{40}Ar				^{38}Ar		^{37}Cl		^{36}Ar

Table 2

Summary of published SW $^{36}Ar/^{38}Ar$ ratios before and after Genesis mission and best estimates of the two calculated as weighted averages. Interestingly, in both cases the most accurate values were obtained in the very first analyses.

SW-collector, mission (reference)	SW $^{36}Ar/^{38}Ar$ ($\pm 1\sigma$)
71501, Apollo Benkert et al. (1993)	5.48 ± 0.05
Kapoeta howardite Becker et al. (1998)	5.58 ± 0.03
Regolith grains, Apollo Palma et al. (2002)	5.80 ± 0.06
Kapoeta howardite Palma et al. (2002)	5.74 ± 0.06
Al-foil, Apollo Geiss et al. (2004)	5.4 ± 0.15
Weighted average before Genesis[a]	5.61 ± 0.02
AloS, Genesis Meshik et al. (2007)	5.501 ± 0.005
BMG, Genesis Grimberg et al. (2008)	5.30 ± 0.13
DOS, Si Genesis Heber et al. (2009)	5.47 ± 0.01
CZ-Si, Genesis Vogel et al. (2011)	5.50 ± 0.01
AuoS, Genesis Pepin et al. (2012)	5.501 ± 0.014
PAC, Genesis (this work)	5.498 ± 0.011
Weighted average after Genesis[b]	5.5005 ± 0.0040

[a] The scatter of the ratios exceeds formally calculated uncertainties indicating a presence of unaccounted systematical errors.

[b] Current best estimate is calculated as a weighted average among most accurate analyses. Only the latest analysis from the Zürich lab is used in the estimation of the weighted average, assuming that two earlier published values measured in BMG and DOS were preliminary.

Table 3

Argon released from PAC solar wind collector in 23-step UV laser ablation combined with subsequent pyrolysis of the laser-ablated area. Atmospheric contamination and blank were removed assuming both have isotopic composition of atmospheric argon (Lee et al., 2006). “R” indicates repeated extraction with the same laser power. Errors are 1σ.

Laser Power, mJ	Total ^{36}Ar, 10^8 at/cm^2	^{38}Ar/^{36}Ar	^{40}Ar/^{36}Ar	SW ^{36}Ar/^{38}Ar	SW ^{36}Ar, 10^8 at/cm^2
0.3	5.1 ± 0.4	.1814 ± .0009	265.8 ± 2.7	8.060 ± 0.528	0.6 ± 0.1
0.5	4.0 ± 0.3	.1789 ± .0011	258.1 ± 2.6	8.509 ± 1.007	0.5 ± 0.1
0.7	8.4 ± 0.5	.1833 ± .0008	270.1 ± 2.5	7.483 ± 0.452	0.8 ± 0.1
0.9	5.6 ± 0.5	.1804 ± .0028	262.2 ± 2.6	8.191 ± 1.203	0.7 ± 0.1
1.1	6.7 ± 0.6	.1818 ± .0009	244.0 ± 2.4	6.581 ± 0.200	1.2 ± 0.1
1.3	3.9 ± 0.2	.1774 ± .0017	129.7 ± 1.3	5.921 ± 0.101	2.2 ± 0.1
1.5	2.2 ± 0.1	.1702 ± .0022	87.2 ± 0.9	6.151 ± 0.112	1.6 ± 0.1
1.8	4.2 ± 0.2	.1744 ± .0017	63.7 ± 0.6	5.863 ± 0.072	3.3 ± 0.2
2	2.8 ± 0.1	.1713 ± .0048	40.7 ± 0.4	5.931 ± 0.194	2.4 ± 0.1
2.4	2.0 ± 0.1	.1559 ± .0021	6.9 ± 0.1	6.447 ± 0.089	2.0 ± 0.1
2.7	8.9 ± 0.4	.1749 ± .0016	1.91 ± 0.03	5.721 ± 0.052	8.8 ± 0.4
3	42.0 ± 1.7	.1729 ± .0007	1.49 ± 0.02	5.786 ± 0.008	41.8 ± 1.7
3.3	24.5 ± 1.0	.1776 ± .0011	3.62 ± 0.03	5.633 ± 0.037	24.2 ± 1.0
3.8	16.7 ± 0.7	.1751 ± .0015	17.5 ± 0.2	5.737 ± 0.053	15.7 ± 0.7
3.8 R	2.1 ± 0.1	.1719 ± .0032	33.0 ± 0.3	5.887 ± 0.123	1.9 ± 0.1
4.2	49.4 ± 2.0	.1811 ± .0010	1.12 ± 0.01	5.522 ± 0.005	49.2 ± 2.0
4.2 R	3.9 ± 0.2	.1820 ± .0020	13.8 ± 0.1	5.505 ± 0.064	3.7 ± 0.2
5	62.4 ± 3.0	.1839 ± .0009	2.38 ± 0.03	5.438 ± 0.006	61.9 ± 3.0
5 R	11.2 ± 0.6	.1986 ± .0019	5.6 ± 0.1	5.030 ± 0.050	11.0 ± 0.6
5 R	9.2 ± 0.5	.2047 ± .0018	7.3 ± 0.1	4.875 ± 0.044	9.0 ± 0.5
6.2	8.2 ± 0.5	.1952 ± .0028	15.1 ± 0.2	5.115 ± 0.078	7.8 ± 0.5
6.2 R	9.3 ± 0.4	.1967 ± .0017	43.0 ± 0.4	5.048 ± 0.052	8.0 ± 0.3
6.2 R	2.4 ± 0.2	.2125 ± .0034	40.6 ± 0.4	4.624 ± 0.087	2.1 ± 0.2
Melt	23.4 ± 1.0	.1972 ± .0031	180.5 ± 1.8	4.751 ± 0.190	9.3 ± 0.5
Total	318.5 ± 4.6	.1829 ± .0004	45.7 ± 0.17	5.498 ± 0.011	269.6 ± 4.3

Table 4

Krypton in aluminum solar wind collectors released in five different laser ablation experiments. Isotopic ratios $^{83}Kr/^{84}Kr$, $^{82}Kr/^{84}Kr$ and $^{80}Kr/^{84}Kr$ were measured twice using different ion collectors. Comparison of these two measurements served as an internal test of multiplier performance. A small fraction of analyses rejected based on this test are not shown here. Blanks represent weighted average of several analyses. Atmospheric values are from Basford et al., 1973.

Sample, extraction method	Area (cm^2)	^{84}Kr, 10^6 at.	$^{86}Kr/^{84}Kr$	$^{83}Kr/^{84}Kr$	$^{82}Kr/^{84}Kr$	$^{80}Kr/^{84}Kr$	$^{78}Kr/^{84}Kr$	$^{132}Xe/^{84}Kr$	Fraction of SW ^{84}Kr	SW ^{84}Kr retrieved 10^7 at/cm^2
A-π/8 (a)	Blank	0.18	0.3067 (95)	0.2134(120)	0.2022 (100)	0.0508 (36)	0.00605 (530)	0.0435		
				0.2014(88)	0.2065 (80)	0.0494 (44)		0.0438		
IR-laser ablation of Al-film on AloS. The beam hits the Al surface at 22.5° angle from normal incident. Y-stage is mounted on X-stage at 22.5°	0.81	11.53	0.3026 (17)	0.2018 (14)	0.2083 (13)	0.0404 (6)	0.00638 (17)	0.0953	0.85	1.21
				0.2036 (13)	0.2042 (11)	0.0410 (7)		0.0966		
	0.72	11.16	0.3039 (11)	0.2032 (11)	0.2022 (10)	0.0403 (4)	0.00632 (19)	0.0899	0.77	1.19
				0.2027 (10)	0.2037 (9)	0.0391 (5)		0.0894		
	0.38	7.26	0.3002 (16)	0.2019 (13)	0.2029 (14)	0.0405 (6)	0.00585 (28)	0.0827	0.65	1.25
				0.2032 (13)	0.2017 (12)	0.0411 (6)		0.0822		
	0.052	0.84	0.3030 (40)	0.2026 (33)	0.2087 (30)	0.0432 (13)	0.00665 (55)	0.0863	0.71	1.15
				0.2041 (32)	0.2065 (30)	0.0386 (14)		0.0856		
A-π/8 (b)	0.96	11.82	0.3004 (19)	0.2046 (19)	0.2053 (16)	0.0393 (6)	0.00652 (22)	0.1019	0.96	1.18
				0.2041 (12)	0.2042 (11)	0.0410 (6)		0.1026		
Same as A-π/8 (a) but made 5 months later under slightly different conditions	3.82	50.23	0.3010 (8)	0.2042 (8)	0.2072 (8)	0.0418 (4)	0.00655 (10)	0.1008	0.94	1.23
				0.2040 (6)	0.2052 (6)	0.0413 (3)		0.1012		
	0.84	14.18	0.3022 (13)	0.2038 (15)	0.2045 (17)	0.0419 (6)	0.00642 (20)	0.0868	0.72	1.21
				0.2044 (12)	0.2044 (12)	0.0408 (5)		0.0884		
	0.32	4.02	0.2999 (23)	0.2014 (18)	0.2068 (17)	0.0415 (7)	0.00652 (35)	0.0982	0.90	1.13
				0.2032 (16)	0.2032 (13)	0.0399 (7)		0.0973		
	Blank	0.19	0.2964 (120)	0.1927 (81)	0.2177 (110)	0.0449 (35)	0.00833 (170)	0.0388		
A-π/4				0.2026 (72)	0.1998 (75)	0.0454 (41)		0.0386		
	3.75	231.4	0.3049 (9)	0.2013 (10)	0.2033 (10)	0.0402 (4)	0.00627 (12)	0.0517	0.17	1.04
				0.2025 (11)	0.2029 (9)	0.0396 (3)		0.0520		

Sample, extraction method	Area (cm^2)	^{84}Kr, 10^6 at.	$^{86}Kr/^{84}Kr$	$^{83}Kr/^{84}Kr$	$^{82}Kr/^{84}Kr$	$^{80}Kr/^{84}Kr$	$^{78}Kr/^{84}Kr$	$^{132}Xe/^{84}Kr$	Fraction of SW ^{84}Kr	SW ^{84}Kr retrieved 10^7 at/cm^2
UV-laser ablation. The laser beam is reflected by 45° dichroic mirror (external to the cell) and hits the Al surface at 45° angle X- and Y stages are moving in the same horizontal plane	0.44	5.63	0.3007 (27)	0.2049 (18)	0.2072 (20)	0.0391 (7)	0.00618 (28)	0.0888	0.75	0.96
				0.2032 (20)	0.2065 (17)	0.0416 (8)		0.0878		
	0.78	12.13	0.3010 (32)	0.2017 (22)	0.2090 (25)	0.0419 (13)	0.00570 (35)	0.0867	0.72	1.12
				0.2030 (23)	0.2052 (21)	0.0423 (10)		0.0867		
	0.15	2.57	0.2987 (35)	0.2018 (25)	0.2081 (29)	0.0397 (11)	0.00621 (44)	0.0797	0.61	1.04
				0.2015 (26)	0.2087 (25)	0.0417 (11)		0.0791		
	0.24	2.97	0.3011 (38)	0.2017 (29)	0.2014 (28)	0.0429 (12)	0.00611 (51)	0.0933	0.82	1.02
				0.2004 (28)	0.2029 (25)	0.0428 (13)		0.0943		
	0.72	10.24	0.3020 (24)	0.2019 (14)	0.2034 (17)	0.0408 (6)	0.00619 (24)	0.0850	0.69	0.98
				0.2023 (18)	0.2023 (15)	0.0403 (5)		0.0854		
A-π	Blank	0.14	0.2913 (140)	0.1916 (95)	0.2039 (110)	0.0420 (48)	0.00535 (580)	0.0554		
				0.1856 (100)	0.1929 (100)	0.0387 (50)		0.0538		
AloS ablated upside down. IR-beam first hits the transparent sapphire substrate and melts Al from the side of the Al-sapphire interface keeping the viewport free of sputtered Al	1.48	20.61	0.3003 (19)	0.2004 (16)	0.2069 (18)	0.0402 (7)	0.00681 (35)	0.0940	0.83	1.16
				0.2003 (16)	0.2056 (16)	0.0411 (7)		0.0958		
	0.20	3.37	0.3038 (50)	0.1993 (49)	0.2043 (42)	0.0385 (22)	0.00665 (63)	0.0836	0.67	1.13
				0.2006 (47)	0.2023 (49)	0.0407 (20)		0.0777		
	0.84	13.50	0.3017 (25)	0.2048 (22)	0.2062 (23)	0.0397 (10)	0.00601 (44)	0.0875	0.73	1.17
				0.2030 (24)	0.2054 (19)	0.0402 (13)		0.0893		
	0.32	3.55	0.3019 (38)	0.2016 (31)	0.2034 (33)	0.0422 (14)	0.00555(130)	0.0985	0.90	1.00
				0.2018 (35)	0.2055 (28)	0.0409 (13)		0.1012		
	0.24	3.38	0.3022 (62)	0.2019 (48)	0.2054 (58)	0.0413 (19)	0.00567 (83)	0.0946	0.84	1.19
				0.2037 (51)	0.2050 (53)	0.0401 (19)		0.0961		
	0.80	10.38	0.3047 (16)	0.2024 (12)	0.2052 (12)	0.0440 (5)	0.00640 (20)	0.0910	0.78	1.02
				0.2036 (13)	0.2074 (12)	0.0409 (5)		0.0912		
P-π/4	Blank	0.38	0.2997(60)	0.1979 (50)	0.2098 (72)	0.0495 (24)	0.00677 (68)	0.0667		

Sample, extraction method	Area (cm^2)	^{84}Kr, 10^6 at.	$^{86}Kr/^{84}Kr$	$^{83}Kr/^{84}Kr$	$^{82}Kr/^{84}Kr$	$^{80}Kr/^{84}Kr$	$^{78}Kr/^{84}Kr$	$^{132}Xe/^{84}Kr$	Fraction of SW ^{84}Kr	SW ^{84}Kr retrieved 10^7 at/cm^2
				0.2035 (52)	0.2063 (48)	0.0456 (25)		0.0685		
PAC ablated by the UV-beam tuned by external 45° mirror. Same as A-π/4 but different collector material: PAC instead of AloS	8.40	98.41	0.3030 (6)	0.2031 (4)	0.2044 (4)	0.0409 (4)	0.00634 (18)	0.0901	0.77	0.90
				0.2021 (4)	0.2039 (4)	0.0421 (4)		0.0905		
	2.04	26.73	0.3013 (9)	0.2042 (7)	0.2049 (8)	0.0411 (3)	0.00631 (30)	0.0839	0.67	0.88
				0.2020 (7)	0.2048 (8)	0.0408 (3)		0.0848		
	0.86	13.84	0.3007 (9)	0.2030 (7)	0.2038 (7)	0.0412 (3)	0.00611 (30)	0.0760	0.55	0.88
				0.2033 (7)	0.2059 (7)	0.0417 (3)		0.0743		
	0.42	8.75	0.3037 (17)	0.2028 (13)	0.2039 (11)	0.0409 (6)	0.00638 (55)	0.0694	0.45	0.93
				0.2018 (13)	0.2029 (11)	0.0419 (6)		0.0702		
Atmospheric Kr			0.3052	0.2014	0.2022	0.0396	0.00609	0.0415		

Notes: Numbers in parenthesis are 1σ. Errors for gas concentrations and elemental ratios are 5–7% based on the scatter observed in series of air standards measured prior and after each experiment. $^{132}Xe/^{84}Kr = 0.041$ was used to resolve SW from trapped Kr.

Table 5

Xenon in Genesis AloS solar wind collectors released in four different laser ablation experiments. Analysis with zero rastered areas are weighted average of several blank analyses.

Sample, extract, method	Area (cm^2)	Total ^{132}Xe, 10^6 at.	^{132}Xe = 1000								Fraction of SW		SW ^{132}Xe retrieved 10^6 at/cm^2
			^{136}Xe	^{134}Xe	^{131}Xe	^{130}Xe	^{129}Xe	^{128}Xe	^{126}Xe	^{124}Xe	$^{84}Kr/^{132}Xe$	^{132}Xe	
A-π/8(a)	0.00	0.01	3004 ± 151	3636 ± 173	<12374	1434 ± 91	10115 ± 280	857 ± 83	n.d.	n.d.	22.9	.100	
	0.81	1.09	3021 ± 36	3736 ± 37	8167 ± 95	1603 ± 25	10440 ± 74	831 ± 19	41.8 ± 4.1	46.4 ± 4.8	10.4	.943	1.26
	0.72	0.98	2967 ± 47	3723 ± 50	8090 ± 145	1641 ± 38	10225 ± 86	811 ± 21	37.0 ± 4.6	54.0 ± 5.6	11.2	.889	1.22
	0.38	0.60	2995 ± 55	3731 ± 61	7859 ± 350	1577 ± 40	10315 ± 97	805 ± 30	39.5 ± 4.9	54.8 ± 8.0	12.1	.829	1.31
	0.052	0.07	2929 ± 135	3649 ± 150	8399 ± 520	1501 ± 93	10410 ± 125	782 ± 71	41 ± 17	50 ± 24	11.6	.863	1.13
A-π/8(b)	0.96	1.20	3029 ± 17	3653 ± 20	8574 ± 66	1621 ± 21	10393 ± 38	863 ± 9	45.7 ± 2.0	56.6 ± 3.0	9.78	.985	1.23
	3.82	4.31	3007 ± 9	3671 ± 11	8238 ± 17	1665 ± 6	10354 ± 19	839 ± 4	42.7 ± 1.1	46.8 ± 1.0	9.90	.976	1.10
	0.84	1.18	3046 ± 15	3754 ± 18	8419 ± 55	1649 ± 12	10377 ± 33	827 ± 8	41.8 ± 2.0	49.2 ± 2.8	11.4	.875	1.23
	0.32	0.43	3030 ± 56	3732 ± 31	8396 ± 84	1613 ± 19	10334 ± 59	872 ± 13	41.9 ± 3.0	50.9 ± 4.1	10.2	.956	1.28
A-π/4	0.00	0.03	3335 ± 410	3754 ± 300	<11423	1937 ± 230	10159 ± 740	791 ± 221	n.d.	n.d.	25.8	−0.093	
	3.75	9.37	3070 ± 35	3737 ± 40	8112 ± 35	1601 ± 22	10055 ± 29	798 ± 9	35.7 ± 2.0	40.6 ± 2.1	19.3	0.340	0.85
	0.44	.500	3011 ± 45	3726 ± 50	8247 ± 93	1607 ± 27	10396 ± 110	818 ± 20	36.0 ± 6.1	46.1 ± 4.5	11.3	0.884	1.01
	0.78	1.02	3060 ± 43	3717 ± 50	8147 ± 48	1640 ± 37	10318 ± 94	796 ± 23	38.1 ± 5.4	54.7 ± 6.8	11.5	0.866	1.13
	0.15	0.20	3079 ± 81	3682 ± 73	8164 ± 108	1613 ± 59	10272 ± 167	830 ± 29	35.9 ± 5.9	51.7 ± 8.0	12.6	0.794	1.08
	0.24	0.26	3087 ± 55	3789 ± 71	8240 ± 98	1633 ± 50	10322 ± 137	833 ± 28	38.0 ± 5.2	45.2 ± 7.3	10.7	0.921	0.98
	0.72	0.87	3023 ± 50	3757 ± 49	8189 ± 62	1609 ± 25	10323 ± 94	814 ± 20	40.1 ± 4.0	50.1 ± 4.8	11.7	0.855	1.03
A-π	0.00	0.02	3203 ± 300	3675 ± 290	<10200	1501 ± 192	10330 ± 560	998 ± 294	n.d.	n.d.	18.3	0.041	
	1.48	1.94	3016 ± 20	3678 ± 51	8184 ± 55	1628 ± 24	10323 ± 19	809 ± 16	40.3 ± 4.2	53.4 ± 1.8	10.5	0.933	1.22
	0.20	0.28	2913 ± 90	3650 ± 94	8408 ± 167	1592 ± 87	10252 ± 30	790 ± 53	48.2 ± 7.4	63.7 ± 9.2	12.4	0.808	1.18
	0.84	1.18	3015 ± 50	3759 ± 48	8268 ± 96	1649 ± 27	10491 ± 96	799 ± 23	39.2 ± 4.7	47.5 ± 4.9	11.3	0.881	1.23
	0.32	0.34	3045 ± 57	3762 ± 68	8438 ± 109	1684 ± 38	10493 ± 23	796 ± 25	44.8 ± 5.5	55.7 ± 6.9	10.0	0.966	1.05
	0.24	0.31	3081 ± 92	3771 ± 97	8436 ± 186	1585 ± 83	10322 ± 22	805 ± 46	42.7 ± 7.5	38.2 ± 9.8	10.5	0.936	1.24
	0.80	0.95	3045 ± 24	3780 ± 20	8116 ± 28	1585 ± 11	10268 ± 37	811 ± 8	36.5 ± 2.0	43.4 ± 1.8	11.0	0.903	1.07
Atmospheric Xe Basford et al. (1973)			3294 (4)	3879 ± 6	7890 ± 11	1513.6 ± 1.2	9832 ± 12	713.6±.9	33.00±.17	35.37±.11			

Notes: Stated errors are 1σ. Errors for gas concentrations and elemental ratios are 5–7% based on the scatter observed in series of air standards measured prior and after each experiment. $(^{84}Kr/^{132}Xe)_{trapped}$ = 24.4 was used to resolve SW from trapped Xe. "n.d." stands for light Xe isotopes in blanks which were too small to be determined.

Table 6

SW-Kr composition and fluences calculated assuming trapped $^{132}Xe/^{84}Kr$ = 0.036 (atmospheric), and $^{132}Xe/^{84}Kr$ = 0.041 (derived from the minimization of the SW-Kr and SW-Xe fluencies scattering).

Sample, extraction method	Assumed Trapped $^{132}Xe/^{84}Kr$	$^{86}Kr/^{84}Kr$	$^{83}Kr/^{84}Kr$	$^{82}Kr/^{84}Kr$	$^{80}Kr/^{84}Kr$	$^{78}Kr/^{84}Kr$	SW ^{84}Kr retrieved, 10^7 at/cm^2
A-π/8 (a)	atm.	.3018 (11)	.2031 (6)	.2047 (6)	.0406 (3)	.00628 (7)	1.23 (9)
	.041	.3018 (11)	.2032 (6)	.2047 (6)	.0406 (3)	.00629 (7)	1.20 (8)
A-π/8 (b)	atm.	.3007 (7)	.2043 (5)	.2060 (4)	.0414 (2)	.00657 (8)	1.20 (14)
	.041	.3007 (7)	.2043 (5)	.2060 (4)	.0415 (2)	.00657 (8)	1.19 (12)
A-π/4	atm.	.3025 (28)	.2033 (22)	.2063 (20)	.0412 (8)	.00658 (37)	1.11 (31)
	.041	.3019 (34)	.2037 (27)	.2072 (25)	.0416 (9)	.00669 (45)	1.02 (11)
A-π	atm.	.3011 (10)	.2021 (9)	.2066 (9)	.0411 (4)	.00644 (25)	1.13 (19)
	.041	.3011 (10)	.2021 (9)	.2067 (9)	.0411 (4)	.00645 (26)	1.11 (18)
P-π/4	atm.	.3015 (6)	.2032 (3)	.2050 (3)	.0420 (3)[b]	.00640 (19)	0.95 (11)
	.041	.3014 (6)	.2033 (3)	.2051 (3)	.0421 (3)[b]	.00641 (19)	0.90 (9)
All data (free fit)		.3010 (22)	.2035 (15)	.2055 (14)	.0413 (7)	.00646 (30)	
All data (fixed trapped comp.)[a]		.3012 (4)	.2034 (2)	.2054 (2)	.0412 (2)	.00642 (5)	1.08 (5)
Diamond[c]		.302 (3)	n.d.	n.d.	n.d.	n.d.	1.22 (10)
Silicon[d]		.303 (1)	n.d.	n.d.	n.d.	n.d.	1.22 (6)
Atm. Kr[e]	.036	.30524 (25)	.20136 (21)	.20217 (4)	.03960 (2)	.006087 (20)	

[a] Weighted average from all data assuming trapped $^{132}Xe/^{84}Kr$ = 0.041.

[b] Polished Aluminum Collector (PAC) $^{80}Kr/^{84}Kr$ is excluded because of the “change of charge” effect.

[c] ETH (Heber et al., 2009).

[d] ETH (Vogel et al., 2011).

[e] From Basford et al., 1973.

Table 7

SW-Xe composition and fluences calculated assuming trapped $^{84}Kr/^{132}Xe$ = 27.7 (atmospheric) and $^{84}Kr/^{132}Xe$ = 24.4 (derived from the minimization of the SW-Kr and SW-Xe fluence scattering).

Sample, extract. method	Assumed trapped $^{84}Kr/^{132}Xe$	$^{136}Xe/^{132}Xe$	$^{134}Xe/^{132}Xe$	$^{131}Xe/^{132}Xe$	$^{130}Xe/^{132}Xe$	$^{129}Xe/^{132}Xe$	$^{128}Xe/^{132}Xe$	$^{126}Xe/^{132}Xe$	$^{124}Xe/^{132}Xe$	SW ^{132}Xe retrieved, 10^6 at/cm^2
A-π/8 (a)	atm.	.2973 (27)	.3716 (29)	.8154 (82)	.1611 (19)	1.0400 (50)	.0827 (14)	.00403 (28)	.00517 (36)	1.26 (7)
	24.4	.2967 (28)	.3713 (29)	.8159 (83)	.1613 (20)	1.0413 (51)	.0829 (14)	.00405 (29)	.00519 (36)	1.23 (8)
A-π/8 (b)	atm.	.3009 (7)	.3680 (8)	.8285 (16)	.1661 (5)	1.0382 (15)	.0847 (3)	.00440 (13)	.00484 (9)	1.22 (8)
	24.4	.3007 (7)	.3678 (8)	.8288 (16)	.1662 (5)	1.0386 (15)	.0848 (3)	.00434 (10)	.00485 (9)	1.21 (7)
A-π/4	atm.	.2996 (24)	.3704 (27)	.8244 (32)	.1636 (16)	1.0358 (42)	.0848 (10)	.00388 (22)	.00494 (24)	1.09 (7)
	24.4	.2987 (25)	.3699 (28)	.8262 (34)	.1641 (17)	1.0433 (48)	.0856 (11)	.00392 (24)	.00509 (27)	1.01 (10)
A-π	atm.	.3008 (15)	.3752 (18)	.8204 (25)	.1612 (10)	1.0399 (14)	.0816 (7)	.00392 (17)	.00497 (13)	1.19 (9)
	24.4	.3003 (15)	.3749 (18)	.8210 (25)	.1614 (10)	1.0409 (14)	.0818 (7)	.00393 (17)	.00499 (13)	1.16 (8)
All data (free fit)		.3015 (38)	.3693 (45)	.8235 (67)	.1652 (30)	1.0408 (70)	.0835 (13)	.00420 (30)	.00494 (31)	
All data (fixed derived trapped component)[a]		.3003 (6)	.3692 (7)	.8263 (13)	.1649 (4)	1.0401 (10)	.0842 (3)	.00417 (9)	.00492 (7)	1.15 (4)
Silicon[b]		.3006 (20)	.3712 (19)	.8163 (28)	.1662 (11)	1.042 (4)	.0818 (49)	n.d.	.00456 (31)	~1.09
Silicon[c]		.2971 (23)	.3667 (35)	.8188 (39)	.1663 (15)	1.045 (5)	.0840 (105)	.00387 (60)	.00449 (50)	1.20 (9)
Diamond[d]		n.d.	n.d.	n.d.	n.d.	1.05 (2)	n.d.	n.d.	n.d.	1.23 (18)
Silicon[e]		n.d.	n.d.	n.d.	n.d.	1.06 (1)	n.d.	n.d.	n.d.	1.25 (7)
Current best estimate[f]		.3001 (6)	.3691 (7)	.8256 (12)	.1650 (4)	1.0405 (10)	.0842 (3)	.00416 (9)	.00491 (7)	1.18 (5)
Atm. Xe.[g] 27.7		.3294 (4)	.3879 (6)	.7890 (11).	.15136 (12)	.9832 (12)	.07136 (9)	.003300 (17)	.003537 (11)	

[a] Weighted average from all Washington Univ. data assuming trapped $^{84}Kr/^{132}Kr$ = 24.4.

[b] Weighted average from two early analysis made at Manchester Univ. (Crowther and Gilmour, 2012).

[c] All Xe analyzes at Manchester Univ. (Crowther and Gilmour, 2013).

[d] ETH (Heber et al., 2009).

[e] ETH (Vogel et al., 2011).

[f] Only recent data from Manchester Univ. are used for the current best estimate since they represent more accurate treatment of essentially the same analyses.

[g] From Basford et al., 1973.

Table 8

Error-weighted mean isotopic deviations (χ^2) of optimized mixtures of fractionated SW, HL[a] and S[b] from Q-gases[c]. First line in each section demonstrates the large difference between SW and Q. Second line correspond to mass fractionated SW without addition of presolar components, which are taken into account in 3-rd and 4th lines. Shown fractions are for major isotopes: ^{84}Kr and ^{132}Xe.

Starting SW-Xe composition	SW-Xe fractionated by (‰)	Xe-HL addition (%)	Xe-S addition (%)	χ^2
Lunar regolith[d,e]	≡ 0	≡ 0	≡ 0	32
	10.5	≡ 0	≡ 0	2.2
	10.2	1.5	≡ 0	0.22
	10.2	1.4	−0.1	0.20
Genesis, Al-collectors[f]	≡ 0	≡ 0	≡ 0	150
	10.9	≡ 0	≡ 0	9.4
	8.1	1.5	≡ 0	1.8
	8.4	1.5	0.15	1.5
Genesis current best estimate (this work)	≡ 0	≡ 0	≡ 0	160
	11.1	≡ 0	≡ 0	10
	8.0	1.6	≡ 0	1.8
	8.2	1.6	0.1	1.6
SW-Kr composition	SW-Kr fractionated by (‰)	Kr-HL addition %	Kr-S addition (%)	χ^2
Lunar regolith[d,e]	≡ 0	≡ 0	≡ 0	63
	8.5	≡ 0	≡ 0	2.2
	6.9	2.6	≡ 0	1.9
	4.3	5.4	0.4	0.8
Genesis current best estimate (this work)	≡ 0	≡ 0	≡ 0	190
	10.2	≡ 0	≡ 0	8.7
	10.1	0.1	≡ 0	8.7
	6.3	4.4	0.4	0.7

[a] Huss and Lewis, 1994.

[b] Productions of s-process isotopes ^{86}Kr and ^{80}Kr are neutron flux and temperature dependent. Ratios ^{86}Kr/^{84}Kr and ^{80}Kr/^{84}Kr vary with the grain size (Lewis et al., 1994). Following Gilmour (2010) we assume the median values of these ratios: 0.83 and 0.02 respectively from the reported ranges of ^{86}Kr/^{84}Kr and ^{80}Kr/^{84}Kr (Ott, 2002).

[c] Busemann et al., 2000.

[d] Pepin et al., 1995.

[e] Similar to minimization made by Gilmour, 2010.

[f] Meshik et al., 2012.